scientific reports

Check for updates

OPEN

Experimental exploring of $Ti_3C_2T_x$ MXene for efficient and deep removal of magnesium in water sample

Shanli Nezami[1], Ahad Ghaemi[1]✉ & Taher Yousefi[2]

In this work, the mechanism and behaviour of magnesium adsorption with $Ti_3C_2T_x$ adsorbent is investigated. $Ti_3C_2T_x$ was synthesized by selective exfoliation of Al layer from Ti_3AlC_2 using acidic solutions of HF 40% and 12 M LiF/ 9 M HCl. The effect of the synthesis method on the structure, the interlayer distance, the type and abundance of the functional groups, the bonds formed, the surface area and the volume of the formed cavities were evaluated by X-ray diffraction, scanning electron microscopy, Energy-dispersive X-ray spectroscopy, Brunauer–Emmett–Teller and fourier transform infrared analyses. The preliminary discontinuous tests of magnesium adsorption with $Ti_3C_2F_x$ and $Ti_3C_2(OH)_x$ in 100 ppm concentration, pH ~ 7.00, ambient temperature and time of 3 h show 182.5 and 99 $mg.g^{-1}$ the adsorption intensity, respectively. The difference in adsorption intensity with $Ti_3C_2F_x$ is the result of the extensive tendency of Mg^{2+} to conduct electrochemical reactions with F^- twice as much as OH^- functional groups. By designing the RSM experiment, analytical, qualitative, optimization and modelling of the magnesium adsorption process with $Ti_3C_2F_x$ adsorbent was carried out with the input variables of magnesium concentration, pH, ambient temperature and time. Isothermal modelling shows the agreement of the experimental results with the Langmuir model and endothermic thermodynamic modelling shows the spontaneity of the adsorption reaction. MXene adsorption–desorption with 0.1 M HCl was done in up to 4 steps. The adsorption results show that $Ti_3C_2F_x$ can show up to 15% initial adsorption intensity by maintaining stability in up to 4 adsorption–desorption steps.

Keywords Ti_3AlC_2, $Ti_3C_2T_x$, HF and HF in situ, Mg^{2+} adsorption, RSM

$Ti_3C_2T_x$ MXene, from the emerging MXenes family, was synthesized for the first time in 2011 by selectively extracting the Al layer from the Ti_3AlC_2 MAX phase. MXenes are identified by the general formula $M_{n+1}X_nT_x$, in which M represents transition metals (such as Sc, Ti, Zr, Hf, V, Nb, Ta, Cr, Mo, and Mn) and n = 1–3. X is carbon, nitrogen, or both, and T_x is surface functional groups (such as O, OH, F, and Cl)[1–3]. MXenes are generally synthesized by selective exfoliation of layer A elements from the 3-dimensional structures of the MAX phase with a hexagonal structure as the starting material. The name "MXenes" is derived from the main phases of MAX with the selective removal of "A" and the addition of "ene" to emphasize the nature similar to 2D materials such as graphene. The MAX phase, a large group of three-dimensional carbides and nitrides with a hexagonal layered structure, reflects the chemical composition $M_{n+1}AX_n$, where "A" is one of the elements III and IV group A. The weaker metal bond in M-A compared to M-X/mixed metal/ion covalent bond facilitates the selective exfoliation of A atomic layers from MAX phases[4–7]. MXenes appear with unique properties compared to their mother phase, i.e., MAX phase, and the most important feature of MXenes is that the properties of MXenes can be controlled by the synthesis method of the selected MAX phase. Electronic, magnetic, optical, mechanical, topological and other properties can be significantly affected by the dimensions and morphology of a material[6,8–12]. Due to the unique two-dimensional(2D) layered structure, hydrophilic surface characteristics, high metallic conductivity, high electrical and thermal properties, and mechanical and excellent chemical stability exhibited by MXenes. Therefore, they are promising candidates for various applications, including energy storage, batteries, electromagnetic interference, shielding, catalysts, optoelectronics, plasmonics, medicine, sensors, etc.[8,13–17]. The intrinsic structure and chemical composition of MXenes originate from transition metals with d-orbital and show attractive physical and chemical properties. The surface of MXenes is covered by

[1]School of Chemical, Petroleum and Gas Engineering, Iran University of Science and Technology, NarmakTehran 16846, Iran. [2]Nuclear Fuel Cycle Research School, Nuclear Science and Technology Research Institute, Tehran, Iran. ✉email: aghaemi@iust.ac.ir

hydroxyl, oxygen, or fluorine; the ratio of these compounds or elements is mainly determined by the synthesis method. The MXene's electrical properties are significantly affected by the surface functional groups resulting from acidic chemical synthesis. Surface functional groups are one of the most attractive features of MXenes that can adjust their properties[8,16,18–20]. The richness of chemistry and surface functional groups of MXenes leads to highly variable and adjustable physical and chemical properties, large elastic modulus, outstanding optical properties, high specific ionic capacity, and compatibility with water and organic solvents[9,21–25]. In addition, research on MXenes for pollutant adsorption has attracted much attention in heavy metal adsorption due to their hydrophilic nature, tunable surface chemistry, and environmentally friendly properties[15,26]. Magnesium is one of the elements of the second group of the periodic table with the symbol Mg, atomic number 12, and has the least reactivity. Magnesium (Mg^{2+}), with a hexagonal crystal structure and soluble in water, is the eighth most abundant element in the earth's crust[27]. Pure and oxide magnesium is used in industry. Mg^{2+} with softness, lack of mechanical stability and high tendency to oxidize is used in lightening missiles, incendiary bombs, weapons fuel and recovery of precious metals such as titanium. Magnesium oxide is used to produce cement, dyes, all kinds of animal feed, refining and purifying waste water and other things[28–30]. Total hardness is the total concentration of Mg^{2+} and calcium ions[31]. Hard water causes many difficulties for industry and washing purposes. Among them, it causes problems in the textile, papermaking and canning industries and the production of deposits in heating devices and steam boilers, which reduces heat transfer, reduces the useful life of components, sometimes shuts down the unit, and finally causes a decrease in production. Also, calcium and Mg^{2+} ions present in water combine with soap and make it insoluble, and by depositing soapy substances, it prevents soap from its main role of cleaning. It is necessary to remove hardness in many cases according to the type of use. Also, one of the causes of death is heart disease, diabetes, nerve failure and corneal problems due to the presence of magnesium in drinking water[31]. Therefore, it is necessary to remove Mg^{2+} from the environment. Among the various technologies for environmental purification from Mg^{2+}, surface adsorption is efficient for environmental purification with advantages such as simplicity of the process, cost-effectiveness, high efficiency, non-degradation of the environment, and production of toxic effluents. Many adsorbents have been used, but their low efficiency and slow kinetics or low selectivity limit their widespread implementation. Therefore, research is being done to develop cost-effective but efficient adsorbents that also have good selectivity[32–34]. The usual methods for removing Mg^{2+} are chemical precipitation or injection of sodium carbonate for Mg^{2+} precipitation and its separation. Chemical precipitation brings several problems such as the need for a large area, problems of increasing pH, poor precipitation, lower efficiency and slow kinetics. The use of a suitable adsorbent with high efficiency and fast kinetics can have an effective performance in removing Mg^{2+} [35,36]. Among the MXenes that have been identified to date, titanium-based MXenes with element abundance, easier synthesis, formation of surface-wide hydroxyl groups during synthesis, no production of toxic products during synthesis, and high chemical and mechanical stability compared to Other MXenes, such as molybdenum or others, have been of more interest for surface adsorption and environmental purification applications. MXene based on titanium has been more successful in the surface adsorption of many heavy metals such as mercury, lead[37], uranium[38], thorium[39], cesium[40], strontium[41,42], and barium[43] compared to other adsorbents such as zeolites, active carbon, MOFs and graphene oxide. In this work, $Ti_3C_2T_x$ is used for magnesium adsorption for the first time. Considering the effect of the synthesis method on the structure, type, and number of surface functional groups, the distance between the layers, the effective specific surface area of MXene, and the volume of the formed cavities, both conventional HF and HF in situ synthesis methods are used for the synthesis of $Ti_3C_2T_x$ from Ti_3AlC_2. to be In the following, the adsorption intensity of each of the MXenes in Mg^{2+} adsorption is investigated and magnesium adsorption by $Ti_3C_2T_x$ is evaluated based on their structure. RSM (CCD) test design is used for qualitative assessment, optimization, modeling, and prediction of Mg^{2+} adsorption process with $Ti_3C_2T_x$ adsorbent. With the help of RSM test design, the effect of independent input parameters such as Mg^{2+}concentration, ambient temperature, time, and solution pH on the output of the adsorption process, i.e., $Ti_3C_2T_x$ adsorbent potential, can be investigated and interpreted based on MXene structure. Finally, the selectivity of the adsorbent in the presence of Mg^{2+}cations in industrial wastewaters and the ability to regenerate the adsorbent were also investigated.

Materials and methods

For the synthesis of Ti_3AlC_2 and $Ti_3C_2T_x$, the materials used are the same as the previous work of Nezami and Ghaemi[39]. $Mg(NO_3)_3.6H2O$ (Mw ~ 254.41 gr/mol), $CaCl_2.2H_2O$ (Mw ~ 147.01 gr/mol), $NaNO_3$ (Mw ~ 84.99 gr/mol), $Fe(NO_3)_3.9H2O$ (Mw ~ 404.00 gr/mol), KNO_3 (Mw ~ 101.10 gr/mol), NaOH (Mw ~ 40 gr/mol) and HNO_3 (Mw ~ 63.01 gr/mol) with a purity 99.99% was purchased from Merck.

Synthesis of Ti_3AlC_2 and $Ti_3C_2T_x$

The synthesis of Ti_3AlC_2 and $Ti_3C_2T_x$ was done by two common methods of HF and HF in situ according to the previous work of Nezami and Ghaemi[39]. Figure 1 shows the synthesis steps of $Ti_3C_2T_x$ from Ti_3AlC_2. Figure 1a shows the contact of the MAX phase with an acidic solution and the breaking of Ti–Al and C-Al bonds. Figure 1b shows the release of Al-F compounds the layering of the accordion structure of the synthesized MXene and the removal of the aluminum atomic layer. Finally, Fig. 1c shows the complete exfoliation of the aluminium atomic layer and the formation of surface functional groups (F^-, OH^- and O^-).

Characterization

Structure and morphology analysis, formation of bonding groups, and analysis of the surface area and volume of cavities with X-ray diffraction analyzes (XRD, STOE, STADI, and MP diffractometer), Scanning electron microscopy (SEM, JSM-7500F FE-SEM, ZEISS EVO 18, Germany), Energy-dispersive X-ray spectroscopy (EDS, JSM-7500F FE-SEM ZEISS EVO 18, Germany), Fourier transform infrared (FTIR, Nicolet Thermos

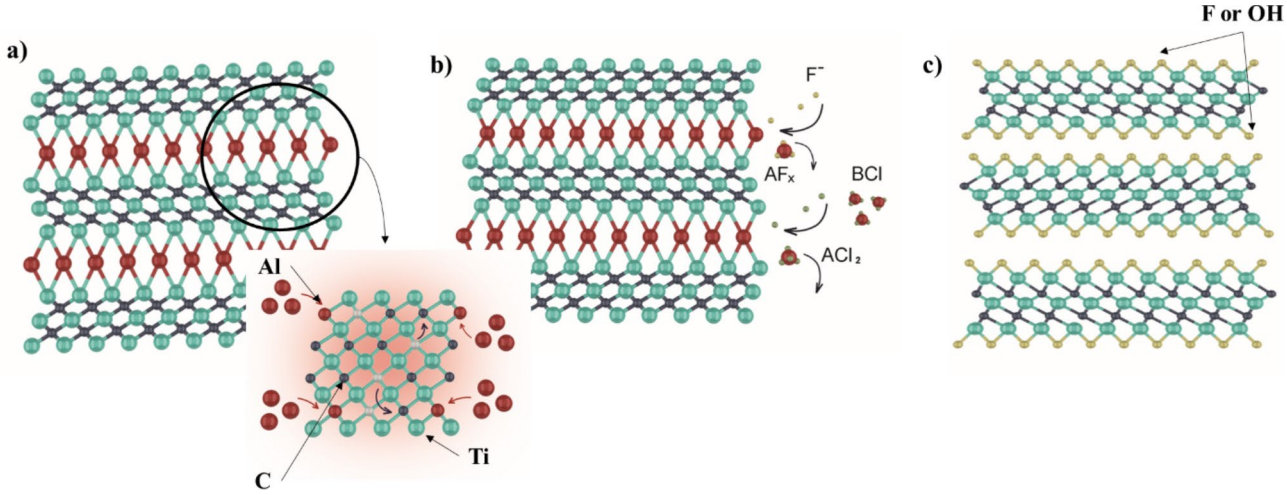

Fig. 1. Synthesis of $Ti_3C_2T_x$ from Ti_3AlC_2.

360 spectrometer), Brunauer–Emmett–Teller (BET, Quantachrome, Nova, 2200) for Ti_3AlC_2, $Ti_3C_2T_x$-HF and $Ti_3C_2T_x$-HF in situ were used. Zeta potential analysis (Nanotrac Wave II, Microtrac, USA) was used to check the pH of the MXene surface. An inductively coupled plasma optical emission spectrometer (ICP-OES, Perkin Elmer, Optima, 7300 DV) is used to analyze the concentration of cations before and after the adsorption process.

Adsorption process

To investigate the effect of functional groups formed on the surface on the adsorption behavior of $Ti_3C_2T_x$-HF and $Ti_3C_2T_x$-HF in situ, discontinuous adsorption experiments were performed at pH ~ 7.00. In the next step, RSM(CCD) test design was used to conduct discontinuous adsorption experiments to investigate the effect of effective parameters on Mg^{2+} adsorption with $Ti_3C_2T_x$. Table 1S shows the investigated parameters along with their upper and lower levels. RSM test design is used for qualitative and analytical investigation Mg^{2+}adsorption process with $Ti_3C_2T_x$, optimization and modeling of the adsorption process, and predicting the effects of Mg^{2+} concentration parameters, ambient temperature, time, and solution pH. The ANOVA statistical method is used to show the relative impact of each input (independent) variable on the output (dependent) variable; here, the adsorption intensity, the effects of interactions, and interferences are used. For this purpose, the F-value test is used in ANOVA analysis. With the help of the F-value test, the influence or lack of influence of the tested parameters and the interaction and interference effects of the tested parameters are evaluated at the confidence level. In addition, the effect of these parameters alone on the output compared to other parameters and the interference effects of the parameters on the output can be well understood. Using Eqs. 1–3, adsorption capacity, qe(mg.g^{-1}), adsorption efficiency R, and distribution coefficient Kd(mg.g^{-1}) were calculated for discontinuous adsorption experiments.

$$q_e = \frac{C_0 - C_e}{m} \times V \tag{1}$$

$$K_d = \frac{C_0 - C_e}{C_e} \times \frac{V}{m} \times 1000 \tag{2}$$

$$R = \frac{C_0 - C_e}{C_e} \times 100\% \tag{3}$$

The initial and final cesium is denoted by C_0 and C_e. M represents the mass of the adsorbent (g) and V represents the volume of the solution (mL)[33,34,39]. 0.1 M NaOH or HNO_3 was used to adjust the pH. ICP analysis is used to analyze Mg^{2+} concentration before and after the adsorption process.

Response surface methodology (RSM)

Experiment design is a suitable solution for identifying effective parameters, initial evaluation of the effect of effective input parameters on the response, identification of the interaction between parameters, modelling by creating a mathematical relationship between parameters and response, and optimizing the process. After selecting the factors, their levels of change and choosing the appropriate response variable, the experimental design is selected according to the objective being pursued. To choose the right test design, you should pay attention to things like randomization, the right number of repetitions, and the number of tests to be done, and finally choose the right design. After designing the appropriate experiment and determining the other explained factors, the experiment is performed based on it, and after the experiment, the answer of each experiment is placed in the desired section. Response Surface Methodology or abbreviated RSM determines the relationship between one (or more) dependent variable and independent variable with a set of mathematical relationships.

Originally, the response surface method was developed for experimental models and then moved to modeling experiments. Response design or RSM is a vortex of statistical techniques that is useful for modeling and analyzing problems where the desired response is affected by several variables, and its goal is to optimize this response. In general, the response surface is a graph of responses. which is presented as a function of one or more factors. Whatever these answers are, the response level method can be done well when the factors and answers change continuously, that is, they have values in a certain range[34,44,45]. To determine the parameters in the estimation of polynomials, the least squares method is used in variance analysis and ANOVA statistical analysis. By using the analysis of variance, the model provided by the response surface method can be evaluated. Analysis of variance is an appropriate method for deciding whether a model is appropriate for response surface method data. In this work, RSM was used to predict, optimize and determine the effective parameters (temperature, time, Mg^{2+} concentration, pH) Mg^{2+} adsorption process from nuclear wastewater. Here, a central composite design (CCD) is used. In the response surface method, an attempt is made to find a way to estimate interactions, quadratic effects, and even the local form of the studied response surface by using a suitable experimental design. In the meantime, certain goals are seriously pursued, the most important of which is improving the process by finding optimal inputs, solving problems and weak points of the process, and stabilizing it. Carrying out the response surface method without having information about the process and the variables affecting it can be misleading. The lower and upper independent variables included in the RSM model are shown in Table 1S.

Results and discussions

Structural morphological details

Figure 2S shows the XRD spectra of Ti_3AlC_2, $Ti_3C_2T_x$-HF and $Ti_3C_2T_x$-HF in situ. The absence of the 104 peaks ($2\theta \sim 39°$) from the Ti_3AlC_2 XRD spectrum in the $Ti_3C_2T_x$-HF and $Ti_3C_2T_x$-HF in situ spectra shows the complete exfoliation of the Al layer[4,46,47]. A significant decrease in Al wt.% in the EDS results (Table 1S) of $Ti_3C_2T_x$-HF and $Ti_3C_2T_x$-HF in situ compared to its initial value in the Ti_3AlC_2 structure confirms the selective and complete peeling of the aluminium layer[48]. The shift of the 002-plane peak ($2\theta \sim 9.815°$) from the Ti_3AlC_2 XRD spectrum to a smaller angle ($2\theta \sim 9.06°$) and ($2\theta \sim 7.745°$), respectively in the $Ti_3C_2T_x$-HF XRD and $Ti_3C_2T_x$-HF in situ spectra, forming a layered structure and it shows the increase in the distance between the layers as a result of the selective exfoliation of the Al layer. The formation of accordion structure and layered $Ti_3C_2T_x$ with both HF and HF in situ synthesis methods is also shown by SEM images (Fig. 2S). In the synthesis with HF in situ, with the Li^+ ions placement and water molecules between the layers, the distance between the layers increases more than in the HF synthesis method. d-spacing = 0.985 nm at $2\theta = 7.745°$ from the spectrum of $Ti_3C_2T_x$-HF in situ and = 0.86 nm d-spacing at $2\theta = 9.06°$ from the XRD spectrum of $Ti_3C_2T_x$-HF in the XRD structural results indicate this theory. SEM images agree with XRD results. The evaluation of the results of SEM (Fig. 3S), EDS (Table 2S) and BET (Figs. 4S, 5S) has been presented in the Nezami and Ghaemi previous work[39]. Synthesis method of $Ti_3C_2T_x$, etchant solution for exfoliation of layer A of Ti_3AlC_2 and its concentration determine the structure and type of functional group formed on the surface of $Ti_3C_2T_x$. Based on the EDS results and the abundance of functional groups formed on the surface as a result of the synthesis method, from now on in this report $Ti_3C_2T_x$-HF will be denoted by $Ti_3C_2F_x$ and $Ti_3C_2T_x$-HF in situ will be denoted by $Ti_3C_2(OH)_x$. Figure 2 shows the FTIR spectra for $Ti_3C_2F_x$-DMSO and $Ti_3C_2(OH)_x$. In both Figs, the peak at 848 cm^{-1} shows the formation of Ti–O-Ti bonds and at 1624 cm^{-1} and 3430 cm^{-1} shows the formation of H-OH. In the $Ti_3C_2F_x$-DMSO FTIR spectrum, the peak of 642 cm^{-1} is the formation of C-F compounds. The peaks at 1624 cm^{-1} and 3430 cm^{-1} in the $Ti_3C_2(OH)_x$ FTIR spectrum are sharper than the $Ti_3C_2F_x$-DMSO FTIR spectrum, which indicates the formation of more H-OH bonds in the HF in situ synthesis method.

The structure of $Ti_3C_2T_x$ layers, the distance between the layers, and the type of functional group formed on the surface (OH^-, O^- & F^-) are effective factors in the adsorption of metal cations by MXene nanolayers. The effect of the type of functional groups in establishing electrochemical interactions with Mg^{2+} adsorption was investigated by conducting discontinuous adsorption experiments[11,25]. Figure 3 shows the Mg^{2+} adsorption intensity with $Ti_3C_2F_x$-DMSO and $Ti_3C2(OH)_x$ at 150 ppm Mg^{2+} concentration, pH ~ 7.00, temperature 298.15 K in a period of 30–240 min. Based on the results obtained from the experimental tests, the Mg^{2+} adsorption intensity with $Ti_3C_2F_x$-DMSO and $Ti_3C_2(OH)_x$ is equal to 185 and 99 $mg.g^{-1}$, respectively. The difference in the structure of $Ti_3C_2F_x$-DMSO and the surface functional groups of $Ti_3C_2F_x$ obtained as a result of synthesis with HF is the main reason for the high intensity of Mg^{2+} adsorption compared to $Ti_3C_2(OH)_x$. From now on, in this report, the process of Mg^{2+} adsorption with $Ti_3C_2F_x$-DMSO adsorbent is investigated.

The high level of Mg^{2+} adsorption with $Ti_3C_2F_x$-DMSO based on EDS results can be interpreted that due to the wide presence of functional group F^- on the surface of the MXene synthesized and the edge of its layers, strong electrostatic attraction force between metal cations Mg^{2+} and F^- functional groups are created, and this attraction power leads to the formation of MgF_2 and ultimately increases adsorption. The electrochemical interaction between Mg^{2+} and F^- functional groups was higher than the electrochemical interaction between Mg^{2+} and hydroxyl groups[10]. Therefore, the effect of parameters of concentration, temperature, time and pH of the environment on Mg^{2+} adsorption intensity with $Ti_3C_2F_x$-DMSO adsorbent is investigated. SEM and EDS results confirm Mg^{2+} adsorption with $Ti_3C_2(OH)_x$ and $Ti_3C_2F_x$-DMSO. In the SEM images, Mg^{2+} adsorbed in the form of white balls is displayed on the surface of both MXenes synthesized. The EDS analysis after the adsorption process shows 12.14 and 15.86 atomic percent for Mg^{2+} in $Ti_3C_2(OH)_x$ and $Ti_3C_2F_x$-DMSO structures, respectively. Figure 4a shows the XRD pattern of $Ti_3C_2F_x$-DMSO before and after Mg^{2+} adsorption. The changes in the peak intensity in the range of $2\theta \sim 36–42°$ indicate the Mg^{2+}adsorption on the F^- groups of $Ti_3C_2F_x$-DMSO. The Fig. 4b illustrates the FTIR of $Ti_3C_2F_x$-DMSO after Mg adsorption. The changes in the intensity of the peak at 642 cm^{-1} related to the C-F bond and the changes in the intensity of the peak at 1642 and 3430 cm^{-1}, which are related to the H-OH bonds, indicate that the Mg^{2+}adsorption by F^- and OH^- occurs on the $Ti_3C_2F_x$-DMSO layers. Meanwhile, the intensity changes of the 642 cm^{-1} peak are more evident[49–52].

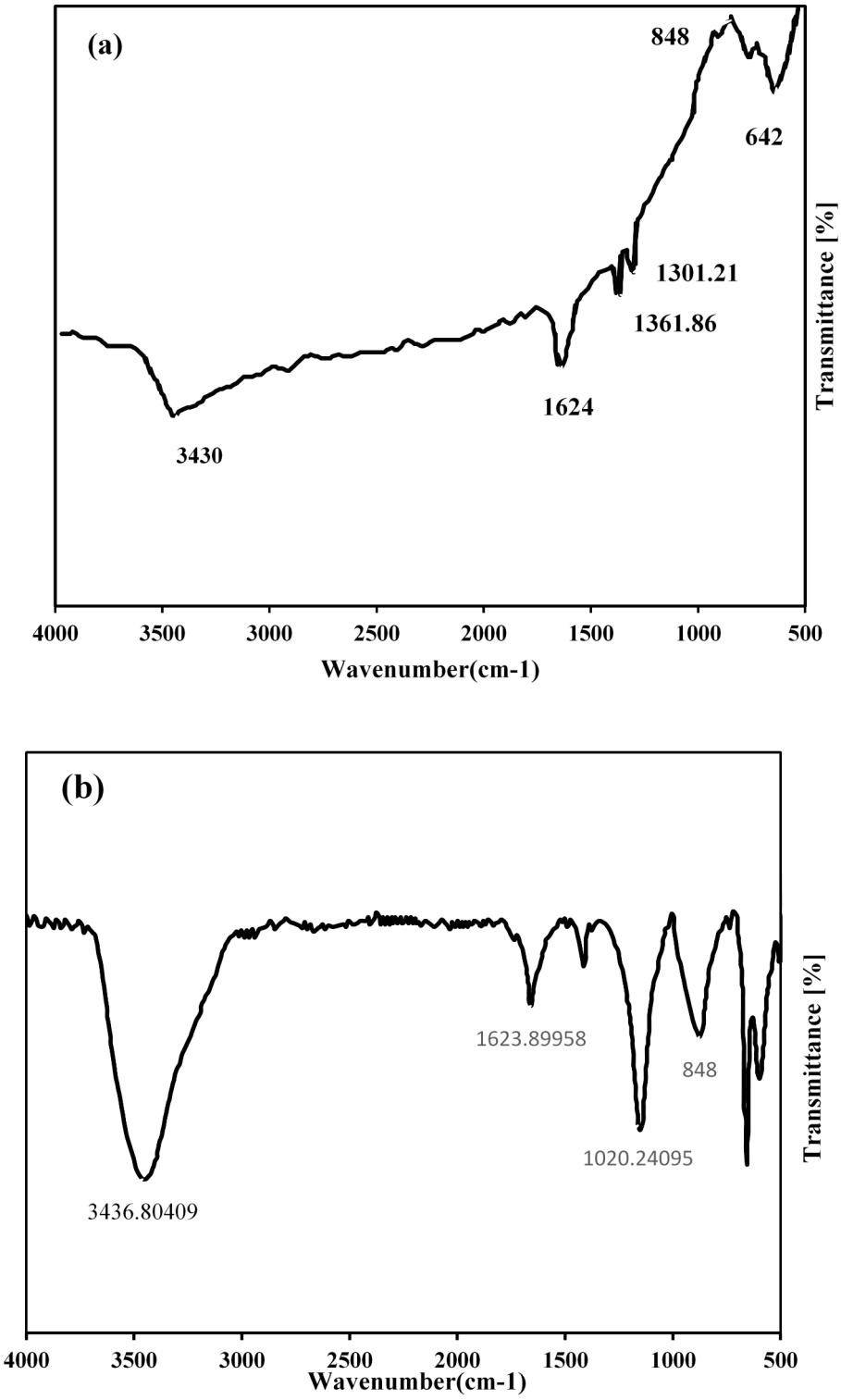

Fig. 2. FTIR (**a**) $Ti_3C_2F_x$-DMSO, (**b**) $Ti_3C_2(OH)_x$.

Adsorbent dose

Adsorbent dosage was investigated on Mg^{2+} adsorption at 150 ppm concentration, temperature 298.15 K, pH ~ 6.0 ± 0.1 and time 180 min at doses of 0.4, 0.6 and 1.2 $g.L^{-1}$. The experimental results (Fig. 5) indicates that by increasing the adsorbent dosage from 0.4 to 0.6 $g.L^{-1}$, the amount of Mg^{2+} adsorption increases. By increasing the adsorbent dosage, the number of surface-active sites and the edge of MXene layers available for Mg^{2+} adsorption increases, so the adsorption increases. As the adsorbent dosage continues to increase from 0.6 to 1.2 $g.L^{-1}$, the adsorption intensity remains constant. At higher values of the adsorbent dose, the

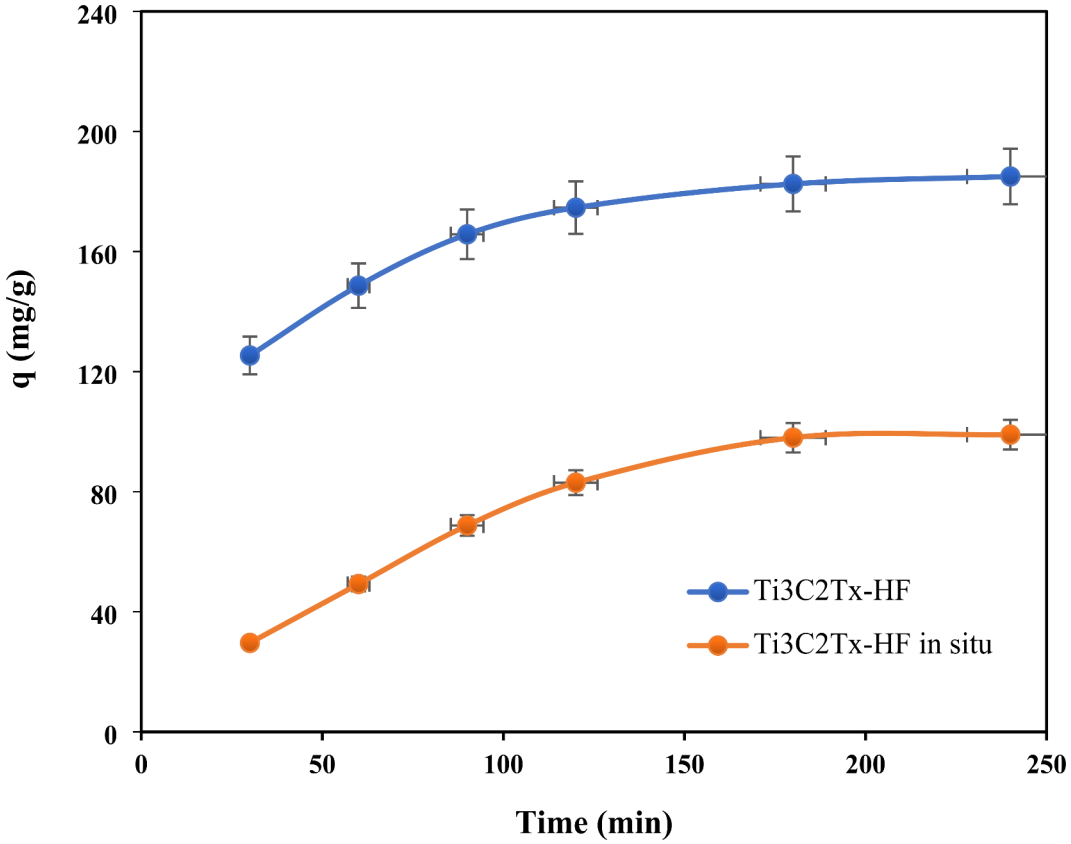

Fig. 3. The effect of the synthesis method on Mg^{2+} adsorption intensity.

amount of adsorption becomes independent of the adsorbent dose. The decrease in adsorption intensity with increasing amount of adsorbent is due to the saturation of adsorption sites during the adsorption process and the accumulation of particles in the high amount of adsorbent, which causes porosity and reduction of its surface area. Therefore based on the Fig. 5, continuous tests of the adsorption process are performed at the adsorbent dose of 0.4 $g.L^{-1}$.

RSM results

In order to model, predict, optimize and select the effective factors (Mg^{2+} concentration, pH, time and temperature) on Mg^{2+} adsorption process with $Ti_3C_2F_x$-DMSO using the responses obtained from 30 RSM experiments, quadratic regression model was used. ANOVA was used to determine the statistical interaction between independent and dependent variables and evaluate the performance of the developed model.The results of the analysis of variance for the $Ti_3C_2F_x$ adsorption parameter model are indicated in Table 3S. The Model F-value of 149.84 implies the model is significant. There is only a 0.01% chance that an F-value this large could occur due to noise. A P-value less than 0.0500 indicates model terms are significant. In this case concentration(A), temperature(B), time (C), AB, BC, A^2, B^2, C^2, D^2 are significant model terms. Values greater than 0.1000 indicate the model terms are not significant. If there are many insignificant model terms (not counting those required to support hierarchy), model reduction may improve your model. The Lack of Fit F-value of 0.47 implies the Lack of Fit is not significant relative to the pure error. There is an 85.34% chance that a lack of Fit F-value this large could occur due to noise. The precision of the built models is indicated by the correlation coefficients (R^2). The R^2 value is 0.9926 in this analysis, which confirms the excellent fit of the data. The R^2 values mean that the proposed models can explain 99.26% of the variance in the adsorption of these participant metallic ions. The Adjusted R^2 showing the model's credibility referred to is 0.9863, which showed that this model was significant. Therefore, the predicted value and adjusted value are in reasonable agreement. The Predicated R^2 of 0.9749 is in reasonable agreement with the Adjusted R^2 of 0.9863; i.e. the difference is less than 0.2. The low C.V percent value of ~ 4.57 shows the model's reliability and repeatability. The R^2 value of more than 0.8 implies a good fit between empirical data and the equations' obtained values. The adequate precision that specifies the signal-to-noise ratio is 48.7333. Adeq Precision measures the signal-to-noise ratio. A ratio greater than 4 is desirable. A ratio of 36.824 indicates an adequate signal. This model can be used to navigate the design space. The $q_{Ti3C2Fx\text{-}DMSO}$ equation is a quadratic model equation for predicting and optimizing the Mg^{2+} adsorption process with $Ti_3C_2F_x$-DMSO and investigating the possible effects of input parameters on the adsorption potential. In this equation, the levels in basic units are specified for each parameter

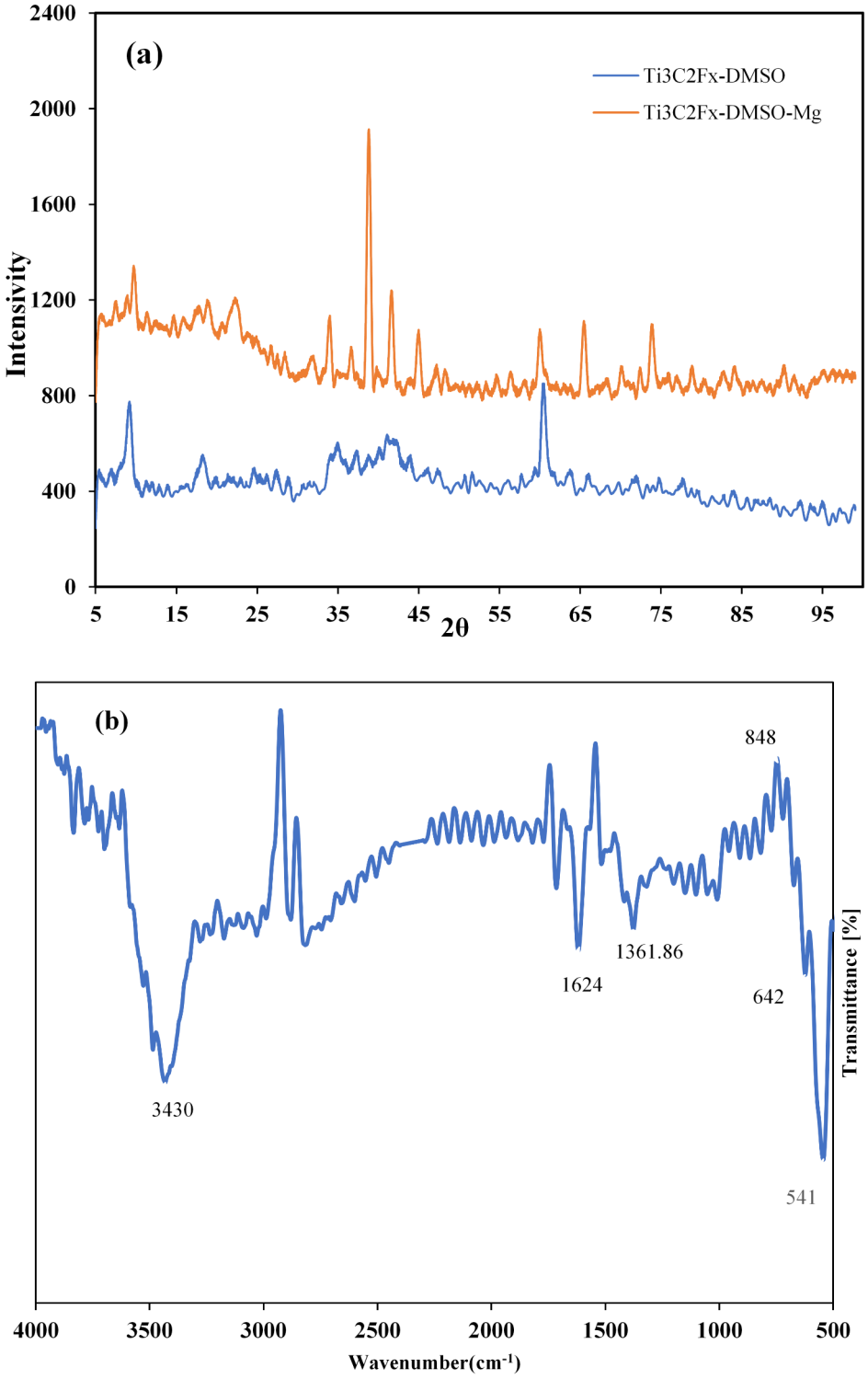

Fig. 4. (**a**) XRD of $Ti_3C_2F_x$-DMSO befor and after Mg^{2+} adsorption, (**b**) FTIR of $Ti_3C_2F_x$-DMSO after Mg^{2+} adsorption.

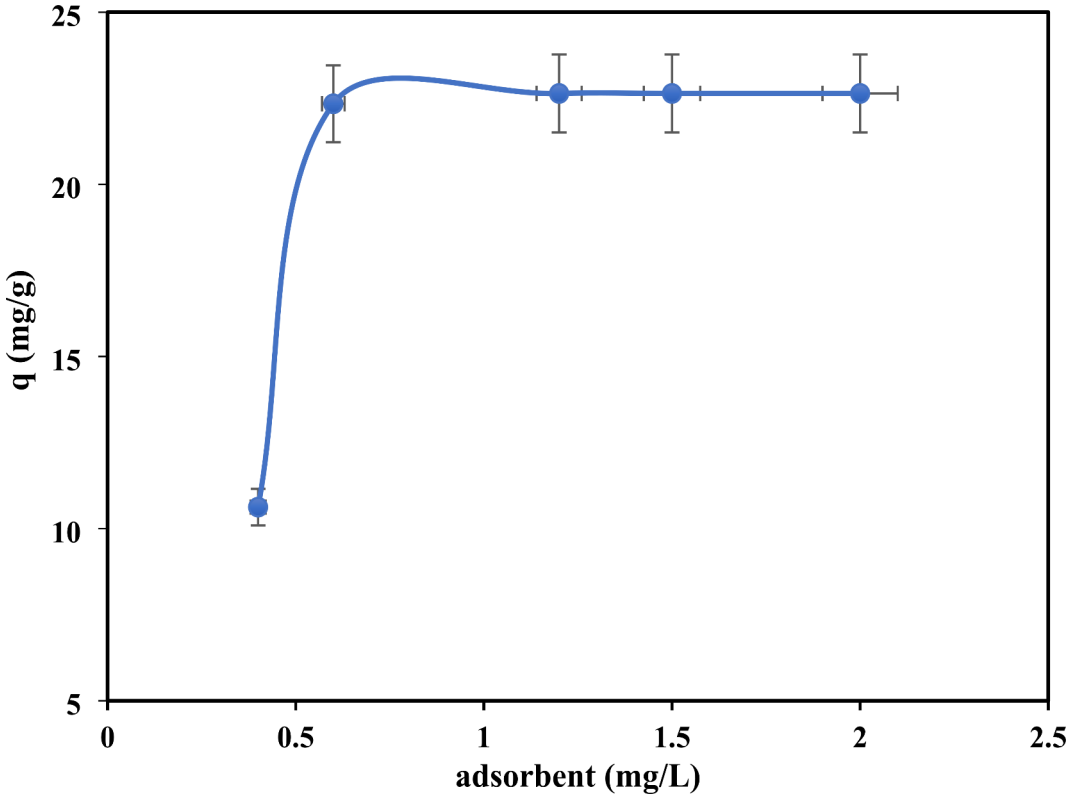

Fig. 5. The effect adsorbent dosage on the Mg^{2+} adsorption intensity with $Ti_3C_2F_x$-DMSO.

$$q_{Ti3C2Fx-DMSO} = -1788.10294 - 82.51998C.C + 37.70489Temp + 12.00879Time - 210.50571pH + 0.281280C.C * Temp - 0.001448CC * Time - 0.046850C.C * pH - 0.034847Temp * Time + 0.949875Temp * pH - 0.031050Time * pH - 0.016383C.C^2 - 0.001732Time^2 - 5.47769pH^2 - 0.108330Temp^2$$

Figure 6S(a) illustrates the approximate normal distribution based on the standardized residual by drawing a straight line through all the data. This straight line has covered almost all the data except for a few cases. In Fig. 6S(b), the experimental values and the predicted values of the model are placed against each other by drawing a straight line. This Fig illustrates the excellent agreement between the experimental values and the values obtained from the model. Therefore, the presented model is very suitable for analytical, and qualitative investigation, predicting the possible effects of each of the independent input parameters (Mg^{2+} concentration, temperature, time and pH of the solution) and the effects of their interactions on the output of the model ($Ti_3C_2F_x$ adsorption intensity). Figure 7S shows the irregular distribution of the predicted values between -2.12132 and 2.12132. Figure 8S Box-Cox plot indicated no need to change the data when the optimal value of Lambda (λ) is between the two red vertical lines. Figure 6 shows the optimal point of the magnesium adsorption process with $Ti_3C_2F_x$-DMSO adsorbent.

Figure 7 shows the graphs obtained from the design of the experiment, the increase in Mg^{2+} adsorption intensity with $Ti_3C_2F_x$-DMSO adsorbent with increasing temperature, Mg^{2+} concentration and time. As the pH solution increases, the adsorption intensity increases and then decreases.

Effect of pH on adsorption capacity

Figure 8 shows the effect of solution pH on the Mg^{2+} adsorption by $Ti_3C_2F_x$-DMSO in the range of 3–11. The pH of the solution increases the chemical connection between the surface-active sites of $Ti_3C_2F_x$-DMSO and Mg^{2+}, the bond between the surface functional groups (F^-) and Mg^{2+} and finally their adsorption by the surface functional groups and the edge functional groups of MXene layers. They affect The ascending-descending trend of Mg^{2+} adsorption by $Ti_3C_2F_x$-DMSO surface active functional groups can be described by changing the surface charge of $Ti_3C_2F_x$-DMSO at different pHs. Since the $Ti_3C_2F_x$-DMSO zeta potential is almost equal to 3, therefore, at pHs lower than this pH, the $Ti_3C_2F_x$-DMSO surface charge is positive. At more acidic pHs (less than 3), the H^+ concentration in the environment is very high. H^+ ion competes with Mg^{2+} for adsorption by F^- surface active groups due to strong electrostatic attraction, and with the positive surface charge of MXene due to the repulsion created between the surface of MXene and Mg^{2+} metal cations, the adsorption rate will be very low. As the pH increases to 7, the H^+ concentration decreases and OH^- increases in the environment. With the increase in the OH^- concentration in the environment and the repulsion between the MXene negative surface charge (F^-)

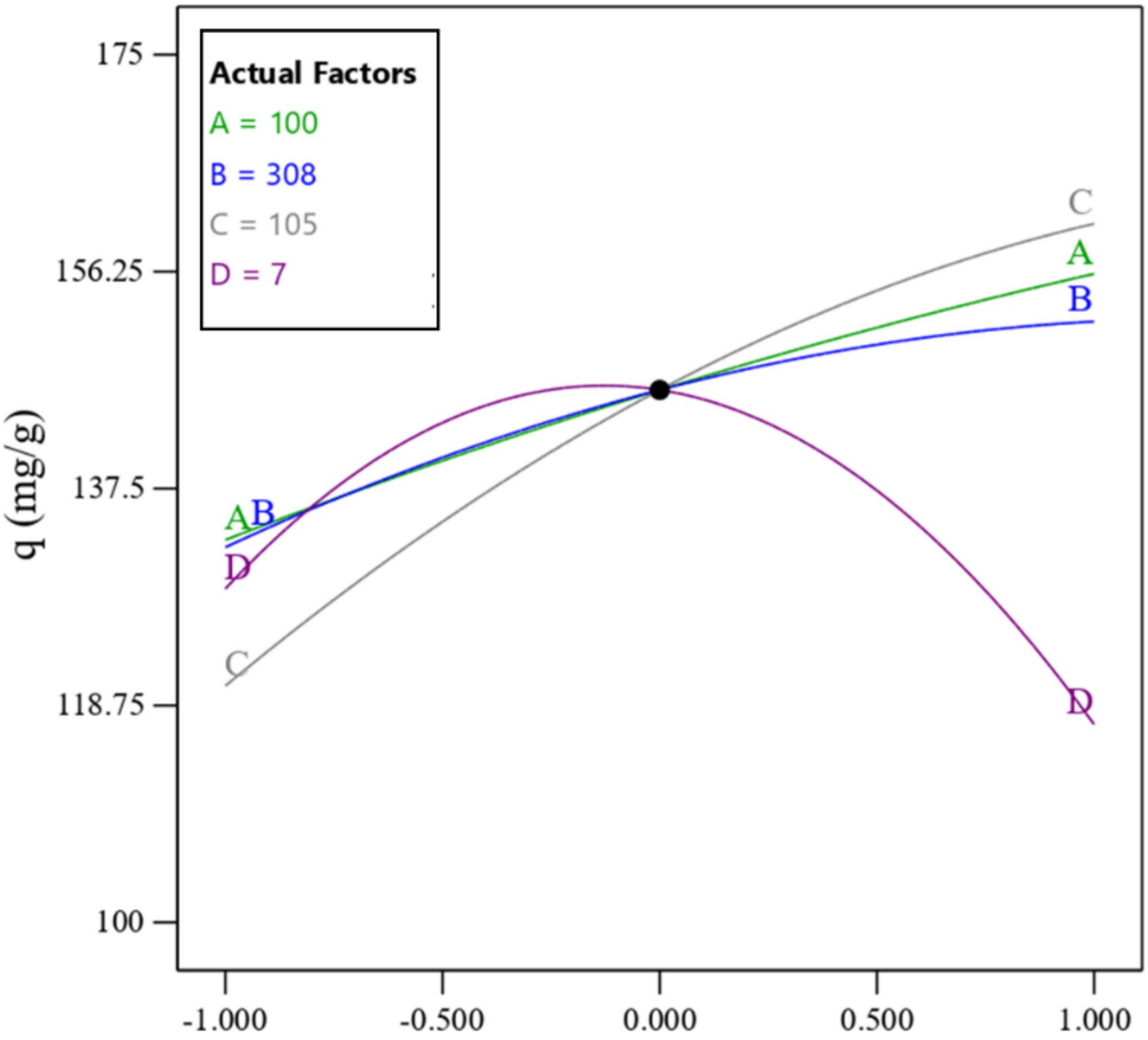

Fig. 6. Deviation from a reference point for $Ti_3C_2F_x$DMSO.

and OH^-, Mg^{2+} cations are easily attracted to the MXene surface charges of and active sites on the edge of its layers with strong electrostatic attraction as a result of attraction[39]. As a result, the adsorption rate increases. As the pH continues to increase from 8 to 11, the adsorption rate decreases. As the pH increases from 8, the OH^- concentration increases, and the high OH^- concentration leads to the hydrolysis of Mg^{2+} in the form of $MgOH^+$ and $Mg(OH)_2$, and as a result, the adsorption rate decreases[37,40].

Thermodynamics of Mg^{2+} adsorption

To evaluate the effect of temperature on the process of Mg^{2+} adsorption with $Ti_3C_2F_x$-DMSO, discontinuous adsorption experiments were performed in the temperature range of 318.15—298.15 K. To investigate the Mg^{2+} adsorption process with $Ti_3C_2F_x$-DMSO as much as possible, it is necessary to conduct thermodynamic studies of the adsorption process by calculating thermodynamic parameters. Thermodynamic parameters reflect the feasibility and spontaneity of processes, endothermic and exothermic reactions and entropy changes during adsorption[53,54]. Thermodynamic parameters include changes in Gibbs free energy (ΔG°), enthalpy (ΔH°) and entropy (ΔS°), which are the most important characteristics of an adsorption process for practical applications. Gibbs free energy is obtained from the following Eq. 4:

$$\Delta G^0 = -RTlnK_d \tag{4}$$

where R is the universal gas constant ($J.mol^{-1}.K^{-1}$), T is the temperature in K and K_d is the constant equilibrium process. The negative values of Gibbs free energy at different temperatures show the spontaneous nature of

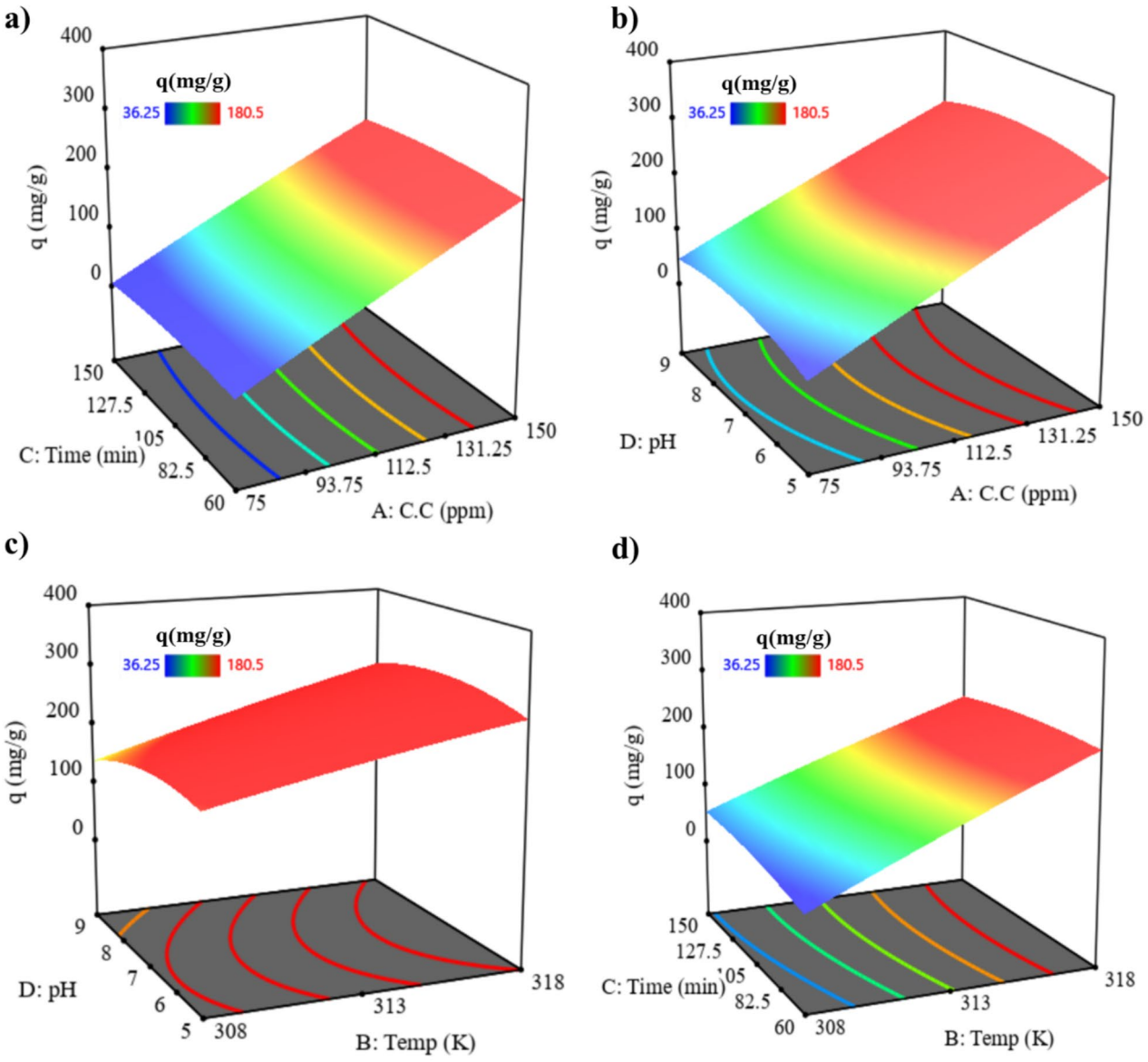

Fig. 7. Surface response effect of Concentration Mg^{2+}, pH, time and temperature on adsorption Mg^{2+} by $Ti_3C_2T_xF_x$-DMSO.

the adsorption process. Figure 9 shows the effect of temperature on Mg^{2+} adsorption intensity with $Ti_3C_2F_x$-DMSO adsorbent and Table 1 shows the thermodynamic parameters values of the Mg^{2+} adsorption process with $Ti_3C_2F_x$-DMSO. The value between -20 and zero indicates physical adsorption and between -80 and -400 in terms of $Kj.mol^{-1}$ means chemical adsorption. The thermodynamic parameters value the ΔH° and ΔS° can be determined by the Van Hoof equation according to Eqs. 5 and 6, respectively, from the slope and width from the origin of the graph drawn $Ln(K_d)$ versus 1/T Calculated.

$$Ln\,(K_d) = \left(\frac{\Delta S^0}{R}\right) - \left(\frac{\Delta H^9}{R}\right) \times \frac{1}{T} \tag{5}$$

$$\Delta G^0 = \Delta H^0 - T\Delta S^0 \tag{6}$$

The $\Delta H > 0$ of Mg^{2+} adsorption with $Ti_3C_2F_x$-DMSO indicates that the adsorption process is endothermic. The $\Delta S > 0$ indicates the increase of irregularity in the adsorbent-adsorbed surface during the process of surface adsorption and the creation of some structural changes in them, which finally shows the irreversibility of the adsorption process.

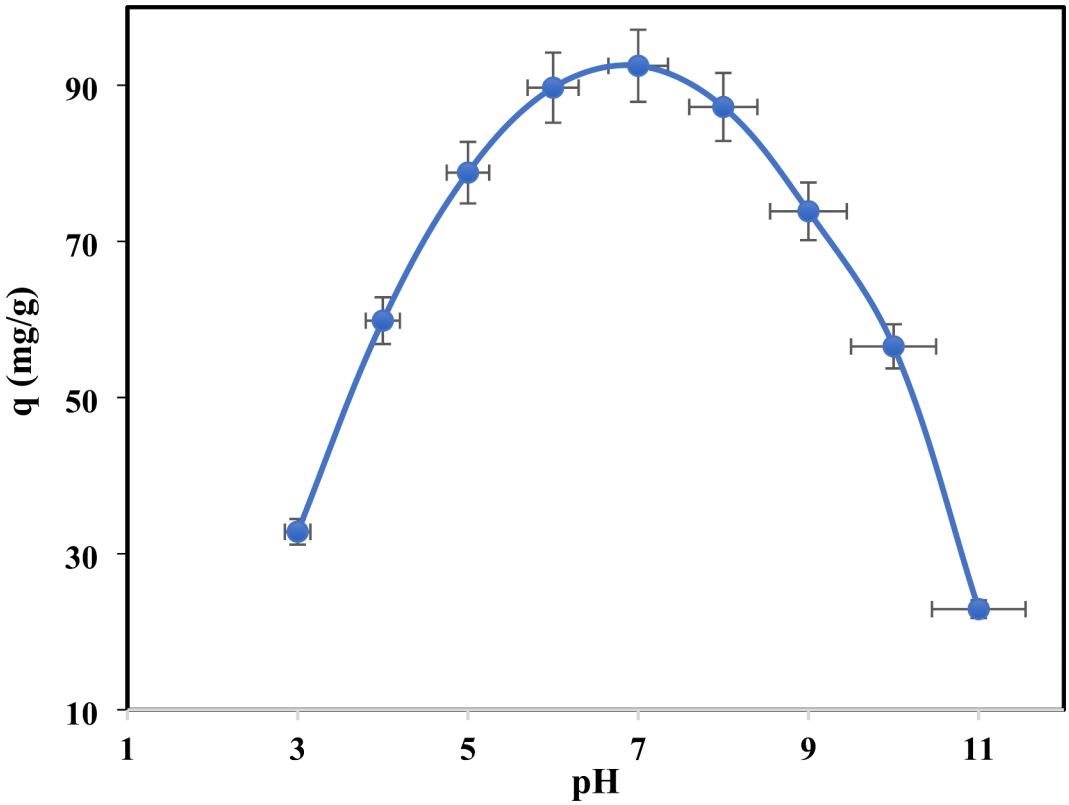

Fig. 8. pH effect on Mg^{2+} adsorption by $Ti_3C_2F_x$-DMSO.

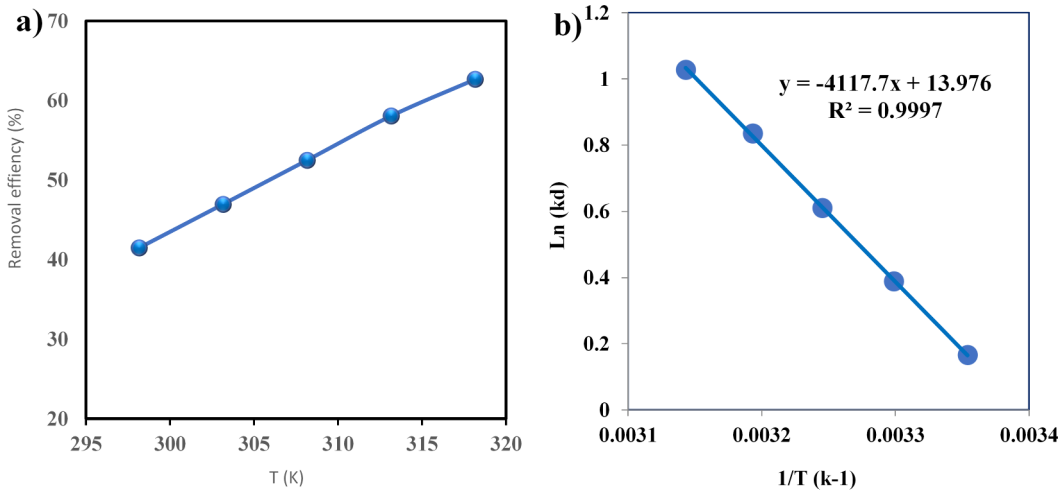

Fig. 9. (**a**) Effect of temperature on the adsorption of Mg^{2+} by $Ti_3C_2F_x$-DMSO, (**b**) Van't Hoff equation plots for the adsorption of Mg^{2+} onto $Ti_3C_2F_x$-DMSO.

$\Delta H^0(kj.mol^{-1})$	$\Delta S^0(j.mol^{-1}.K^{-1})$	$\Delta G^0(kj.mol^{-1})$				
		298.15 K	**303.15 K**	**308.15 K**	**313.15 K**	**318.15 K**
154.666	542.53	-316.279	-318.989	-321.699	-324.409	-327.12

Table 1. Thermodynamic parameter from fitting results of Mg^{2+} adsorption by $Ti_3C_2F_x$-DMSO.

Adsorption isotherms

To model the adsorption isotherm, discontinuous Mg^{2+} adsorption experiments were designed and performed with $Ti_3C_2F_x$-DMSO adsorbent in the 50–150 $mg.g^{-1}$ concentration range. The obtained experimental results(Fig. 10) show that with the increase of the initial concentration, the Mg^{2+} adsorption intensity with $Ti_3C_2F_x$-DMSO adsorbent increases.

The mechanism of Mg^{2+} adsorption with $Ti_3C_2F_x$-DMSO was evaluated by Langmuir, Freundlich, and Dubinin-Radushkevich isotherm models. The Langmuir isotherm model assumes that adsorption occurs in special homogeneous places inside the adsorbent. In the Langmuir isotherm, it is assumed: (1) the adsorption process occurs as a single layer adsorption (chemical adsorption); (2) the surface of absorbent pellets or any adsorption site is homogeneous; and, (3) heat of adsorption does not change with coating. In other words, according to the Langmuir isotherm, adsorption occurs when a free adsorbing molecule collides with an unoccupied adsorption site and each absorbed molecule does the same amount of repulsion. The value of $(L.m^{-1}g^{-1})b$ is the Langmuir constant and is related to the free energy of adsorption. Despite the reversible adsorption nature of the Langmuir model, sometimes this model fits irreversible adsorption[55]. Equation 7 shows the general formula of the Langmuir model:

$$\text{Langmuir}: \quad q_e = \frac{q_m K_l C_e}{1 + K_l C_e} \tag{7}$$

Freundlich isotherm, another adsorption model, does not have many limitations compared to Langmuir isotherm, in other words, it can be used for both homogeneous and heterogeneous surfaces, and both physical and chemical adsorption. Equation 8 shows the general form of the Freundlich equation. In this equation, Langmuir's constant K_f is a constant related to adsorption capacity and 1/n is an experimental parameter related to adsorption intensity, which changes with the degree of material heterogeneity[55].

$$\text{Freundlich}: \quad q_e = k_F C_e^{1/n} \tag{8}$$

The Dubinnin-Radushkevich model is more general than the Langmuir model and does not assume adsorption on a homogeneous surface with constant adsorption energy. This model distinguishes between physical and chemical adsorption. Equation 9 shows the Dubinnin-Radushkevich model[55].

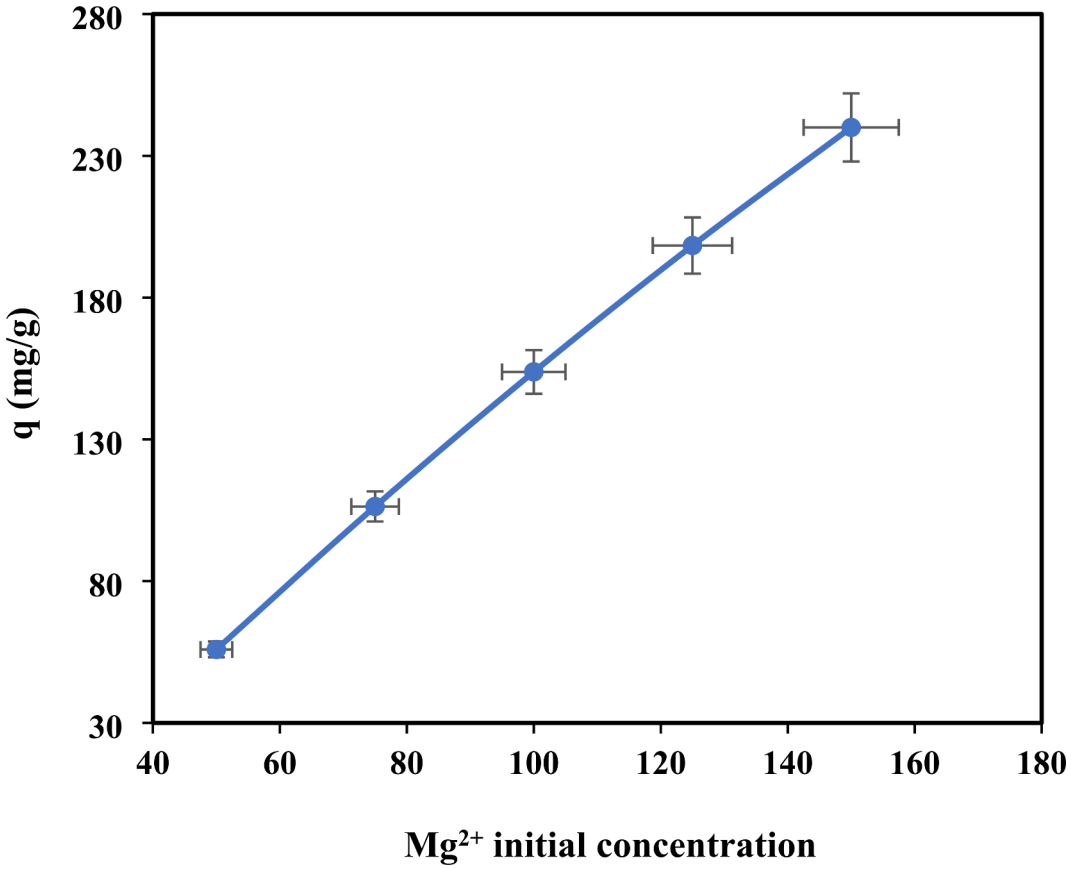

Fig. 10. Effect of Mg^{2+} concentration on the adsorption by $Ti_3C_2F_x$-DSMO.

$$\text{Dubinin} - \text{Radushkevich}: \quad q_e = q_s \exp\left(-k_{ad} \times E_a^2\right) \tag{9}$$

Table 2 presents the adsorption isotherm parameters for Mg2 + adsorption with Ti3C2Fx-DMSO. Three isotherm models, including Langmuir, Freundlich, and Dubinin-Radush isotherm models, were applied for the process modeling. The results showed that the R2 value for the Langmuir isotherm model indicates the homogeneous adsorption of Mg2 + on sites with the same energy (F—functional groups)[25,46,47].

Figure 11 respectively show the isotherm diagrams related to the Mg^{2+} adsorption with $Ti_3C_2F_x$-DMSO, and the experimental data are in complete agreement with the modelling.

The Table 3 presents the studies performed for the Mg^{2+} adsorption with the adsorbents that have been investigated so far. So far, active carbon, MOF, graphene oxide, and similar adsorbents have not been used for Mg^{2+} adsorption. In addition to the adsorbents presented in the table below, in 2019 the Mg^{2+} adsorption from salt water, with solvent extraction, 81% of Mg^{2+} is absorbed during 3 continuous stages[56,57].

Kinetics adsorption

Figure 3 shows the time effect of Mg^{2+} adsorption with $Ti_3C_2F_x$-DMSO up to 240 min. The Mg^{2+} adsorption process with $Ti_3C_2F_x$-DMSO happens in two stages. In the first 90 min, the Mg^{2+} adsorption occurs, which is the fastest stage. In the first 90 min, according to the availability of surface active groups (F^-, O^-, and OH^-(to a lesser extent)), by establishing electrochemical interactions between dissimilar charges, Mg^{2+} is quickly adsorbed on the $Ti_3C_2F_x$-DMSO surface sits. The second stage is slower than the first stage. At this stage, by filling the surface-active sites with a negative charge, adsorption on the surface-active sites, and adsorption on the edge sites of the layers takes place. By using DMSO for the intercalation process, the distance between the layers is increased and it is possible to absorb and establish electrochemical interactions between magnesium cations and surface-active groups[61]. Kinetic adsorption models are used to check adsorption intensity. In addition to the optimal time, kinetic studies also show the reaction mechanism through kinetic modelling. Three pseudo-first-order (PFO), pseudo-second-order (PSO), Ritchie Second Order (RSO) and Elovich kinetic models were used to study the adsorption (Eqs. 10–13).

$$q_t = q_e \times (1 - exp\,(-k_1 t)) \tag{10}$$

$$q_t = \frac{k_2 q_e^2 t}{1 + k_2 q_e t} \tag{11}$$

$$q_t = q_e - \frac{q_e}{1 + k_2 t} \tag{12}$$

$$q_t = \beta * ln\,(\alpha\beta) + \beta ln\,(t) \tag{13}$$

Table 4 shows the results of kinetic models for Mg^{2+} adsorption with $Ti_3C_2F_x$-DMSO adsorbent. R^2 PSO model compared to R^2 PFO and Elovich models shows the agreement of experimental data with PSO kinetic model. $K_2 = 0.00024$ indicates that the Mg^{2+} adsorption by $Ti_3C_2F_x$-DMSO is slow. On the other hand, the F^- active sites on the $Ti_3C_2F_x$-DMSO adsorbent shows the compatibility of the Mg^{2+} adsorption kinetic model with maxin. Despite the equality of R^2 PSO model with R^2 RSO model, the RSO kinetic model for Mg^{2+} adsorption by $Ti_3C_2F_x$-DMSO cannot be presented. The RSO model refers to the adsorption on the adsorbent, while the adsorption of Mg^{2+} with $Ti_3C_2F_x$-DMSO occurs by surface active sites[62].

Figure 12 shows the kinetic diagram obtained from the $Ti_3C_2F_x$-DMSO model, which is in complete agreement with the diagram obtained from the experimental results.

MXene	Model	Parameters	
$Ti_3C_2F_x$-DMSO	Langmuir	q_m (mg/g)	94.51309
		K_l	0.00
		R^2	0.9993
		AARE%	0.1084
	Freundlich	K_l	0.531
		R^2	0.9874
		n	0.817
		AARE%	0.0442
	Dubinin-Radushkevich	q_s (mg/g)	283.433
		Beta	855.962
		Ea	0.024
		R^2	0.9809
		AARE%	0.1194

Table 2. Isotherm parameters fitted by Langmuir and Freundlich models for Mg^{2+} adsorption onto $Ti_3C_2F_x$-DMSO.

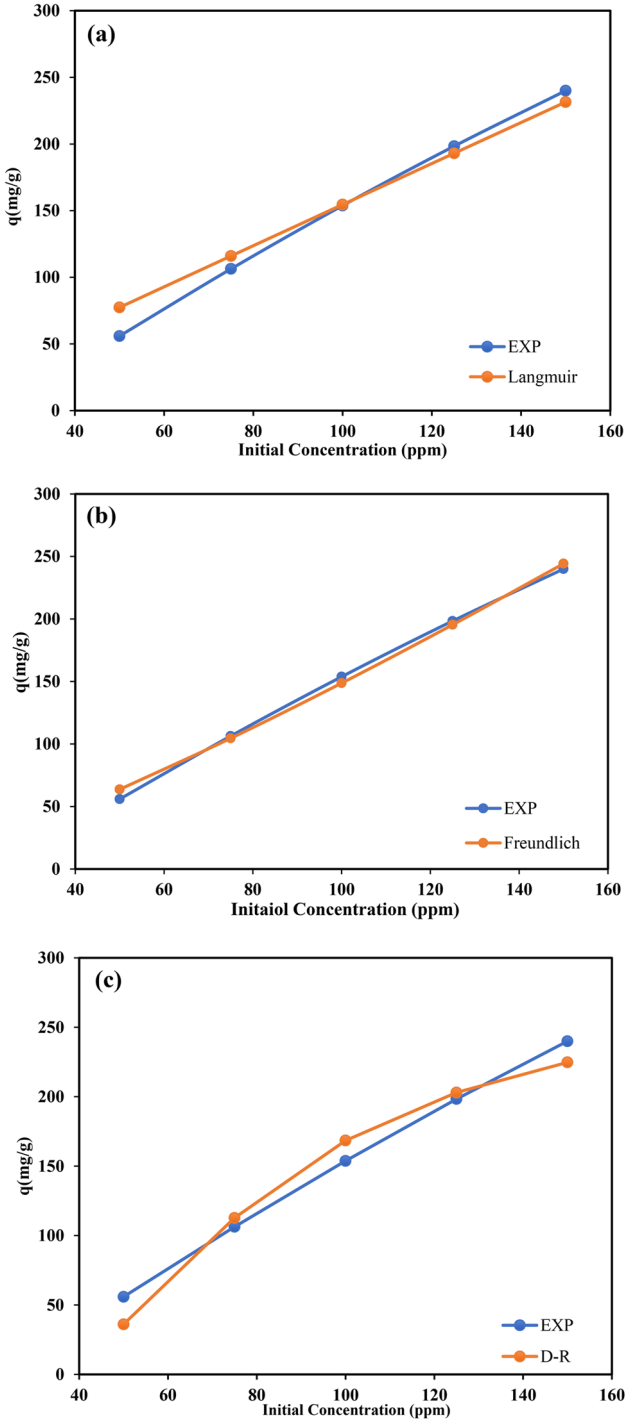

Fig. 11. Comparison of the experimental data results with the isotherm models; (**a**) Langmuir, (**b**) Freundlich and (**c**) R-D regarding the Mg^{2+} adsorption by $Ti_3C_2F_x$-DMSO.

Reduction of $Ti_3C_2F_x$-DMSO

To investigated the regeneration capability of the adsorbent, 0.5 g of $Ti_3C_2F_x$-DMSO was used. The experimental test of Mg^{2+} adsorption with $Ti_3C_2F_x$-DMSO was carried out under the operating conditions of 100 ppm Mg^{2+} concentration, a temperature at 298.15 K, the time of 100 min, and pH of ~ 7.0 ± 0.1. 0.1 M HCl was used to regenerate the spent adsorbent. After the adsorption process, the used adsorbent was stirred with 10 ml of 0.1 M HCl for 30 min at room temperature. After 30 min, the supernatant solution was separated with the help of a centrifuge at 3500 rpm, and until the surface pH of MXene reached pH ~ 6.0 ± 0.1, the surface of MXens was washed with deionized distilled water. Finally, after the MXene surface pH reaches 6, the adsorbent is collected by vacuum filtration and 0.45 µm PVDF membrane filter and heated for 2 h in a vacuum oven to dry at temperature of 353.15 K. This process was done 3 times, except for the first stage adsorption, and the amount

Adsorbent	Reaction condition					q_{max} (mg/g)	Isotherm	Kinetics	Mechanism	Ref
	m/V (gr/L)	C_0 (ppm)	pH	Time (min)	Temp (K)					
Chitosan powder	0.1	100	7	120	RT	174.9	Langmuir	-	-	58
Chitosan beads						422.6				
Pumice	10	20	6	180	RT	44.53	-	-	-	59
Pumice-Modified						56.11				
Poly acrylic Acid	0.20	400	7	120	RT	196.1	-	-	-	60
$Ti_3C_2F_x$-DMSO	0.4	100	7	240	RT	185.0	Langmuir	FSO	Complexation Electrostatic interaction	This Work

Table 3. Summary of Mg^{2+} adsorption.

MXene	Model	Parameters	
$Ti_3C_2F_x$-DMSO	PFO	q_e (mg/g)	178.80
		K_1	0.03515
		R^2	0.99497
	PSO	q_e (mg/g)	204.33
		K_2	0.00024
		R^2	0.99919
	RSO	q_e (mg/g)	204.33
		K_2	0.04903
		R^2	0.99919
	Elovich	Alfa	1.15
		Beta	0.000
		R^2	0.99784

Table 4. Kinetics model parameters and correlation coefficients for Mg^{2+} sorption on $Ti_3C_2F_x$-DMSO.

of Mg^{2+} concentration remaining after adsorption in the solution was checked by ICP. To check the stability MXene structure and functional groups, FTIR and SEM analysis were performed after 4 steps of adsorption and desorption[39,63].

The Fig. 13 indicates the experimental results of the adsorption and desorption process of $Ti_3C_2F_x$-DMSO. The results of the first adsorption show that part of the surface active sites and the edge of the MXene layers are covered by Mg^{2+}. In the same way, in reuse for the second adsorption, the percentage of adsorption occurs. The results indicated that after the reduction of $Ti_3C_2F_x$-DMSO, its adsorption intensity returns to its first level. As a result of reduction with HCL, Mg^{2+} is easily replaced by H^+, which is due to the smaller hydration radius of H^+ compared to Mg^{2+}. After reduction, $Ti_3C_2F_x$-DMSO can be used for 4 adsorption cycles without an obvious decrease in adsorption intensity.

Figure 14 shows SEM and EDS structural analyses before and after 4 adsorption–desorption steps. SEM images show that the accordion and layered structure of MXene has not changed after 4 adsorption–desorption steps, and the reduction of F^- functional groups as a result of washing with acid is the main reason for the decrease in adsorption intensity.

Adsorption mechanisms

XRD, SEM, EDS and FTIR analyzes have been performed to identify the chemical and physical changes of $Ti_3C_2F_x$-DMSO adsorbent after Mg^{2+} adsorption. In Fig. 14, SEM images after the adsorption process confirm the stability of the structure and the Mg^{2+} ions presence on the $Ti_3C_2F_x$-DMSO layers. Strong electrostatic interactions between Mg^{2+} and F^- ions on the surface of the adsorbent lead to the formation of strong surface complexes and Mg^{2+} adsorption on the $Ti_3C_2F_x$-DMSO adsorbent. On the other hand, the investigation and studies of the effect of pH on Mg^{2+} adsorption show that electrostatic interactions strongly affect Mg^{2+} adsorption. Therefore, complex formation and electrostatic interaction are the dominant mechanisms in the Mg^{2+} adsorption with $Ti_3C_2F_x$-DMSO[61,64] (Fig. 15).

Selectivity test

The selectivity of Mg^{2+} adsorption by $Ti_3C_2F_x$-DMSO adsorbent in the presence of Ca^{2+}, Fe^{3+}, K^+ and Na^+ cations at 50, 100 and 150 ppm concentrations under operating conditions of ambient temperature, pH ~ 7.0 and contact time 3 The watch was checked. The experimental results (Fig. 16) show that the Mg^{2+} adsorption with an ionic radius of 0.16 nm is higher than calcium, sodium and potassium cations with an ionic radius of 0.197, 0.147 and 0.227, respectively. Among the examined cations, potassium adsorption intesity is lower with the lowest electronegativity (0.82) and larger ionic radius. The adsorption intensity of calcium and sodium, having lower electronegativity, is 0.1 and 0.93, respectively, compared to Mg^{2+} with 1.31 electronegativity. Among the cations, iron with the smallest ionic radius (0.136 nm) and the highest electronegativity (1.83) exhibits the

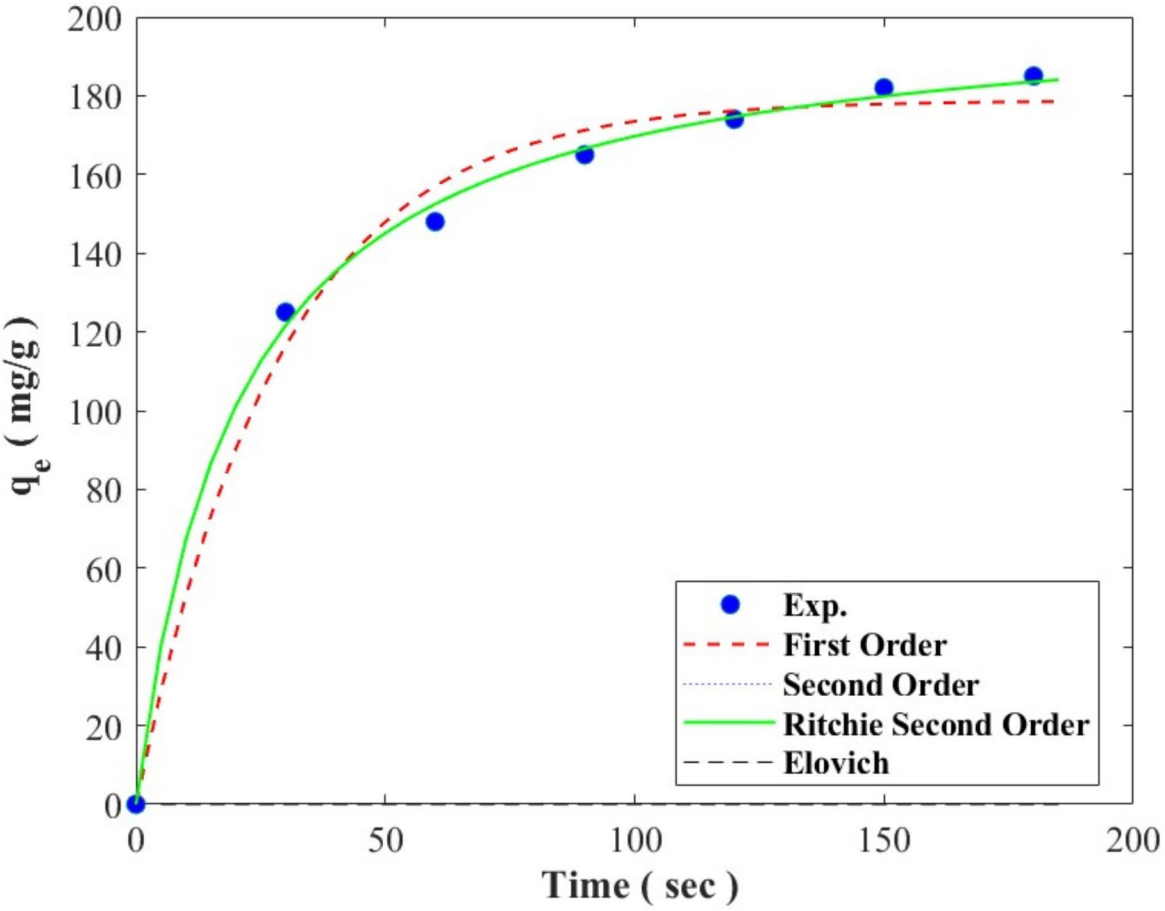

Fig. 12. Kinetic models Mg^{2+} sorption by $Ti_3C_2F_x$-DMSO.

highest adsorption with $Ti_3C_2F_x$-DMSO adsorbent. The Fe^{3+} adsorption intensity is higher than that of Mg^{2+} and it shows that there is a tendency to adsorb trivalent cations for $Ti_3C_2F_x$-DMSO adsorbent.

Conclusion

Surface functional groups are one of the most attractive features of MXenes, whose type and abundance are determined as a result of the synthesis method. Surface functional groups lead to changes in physico-chemical properties and variable effectiveness of MXenes in adsorbing heavy metals. The formation of different surface functional groups, as a result of the common synthesis methods of HF and HF in situ and the larger volume of cavities in the synthesis with HF in situ, can be effective in the adsorption performance of the synthesized $Ti_3C_2T_x$. Discontinuous adsorption experiments show extensive electrochemical reactions between Mg^{2+} and F^- compared to O^- (OH^-) functional groups. The approximate equality of the specific surface area of $Ti_3C_2T_x$ in both synthesis methods and the greater interlayer spacing of $Ti_3C_2T_x$-HF in situ distinguish the potential effect of surface functional groups. Langmuir isotherm modeling results, monolayer adsorption on homogeneous sites, and thermodynamic modeling results show the feasibility, spontaneity and exothermicity of Mg^{2+} adsorption process with $Ti_3C_2F_x$-DMSO adsorbent. pH is one of the most important parameters affecting the protonation and deprotonation of MXene surface and the intensity of Mg^{2+} adsorption. With the increase of pH ~ 7.00, the Mg^{2+} adsorption intensity increases up to 240 $mg.g^{-1}$. As the pH continues to increase, the adsorption intensity decreases with Mg^{2+} hydrolysis. The kinetic modeling results show that the PSO model with R^2 above 0.9999 is in perfect agreement with the experimental data. Langmuir isotherm modelling results, monolayer adsorption on homogeneous sites, and thermodynamic modelling results show feasibility, spontaneity and endothermicity of Mg^{2+} adsorption process with $Ti_3C_2F_x$-DMSO adsorbent. Appropriate selectivity, ability to regenerate the adsorbent and its efficiency up to 4 stages of adsorption–desorption while maintaining the stability of the adsorbent show that $Ti_3C_2F_x$-DMSO can be used as a potential adsorbent in the Mg^{2+} purification of the environment.

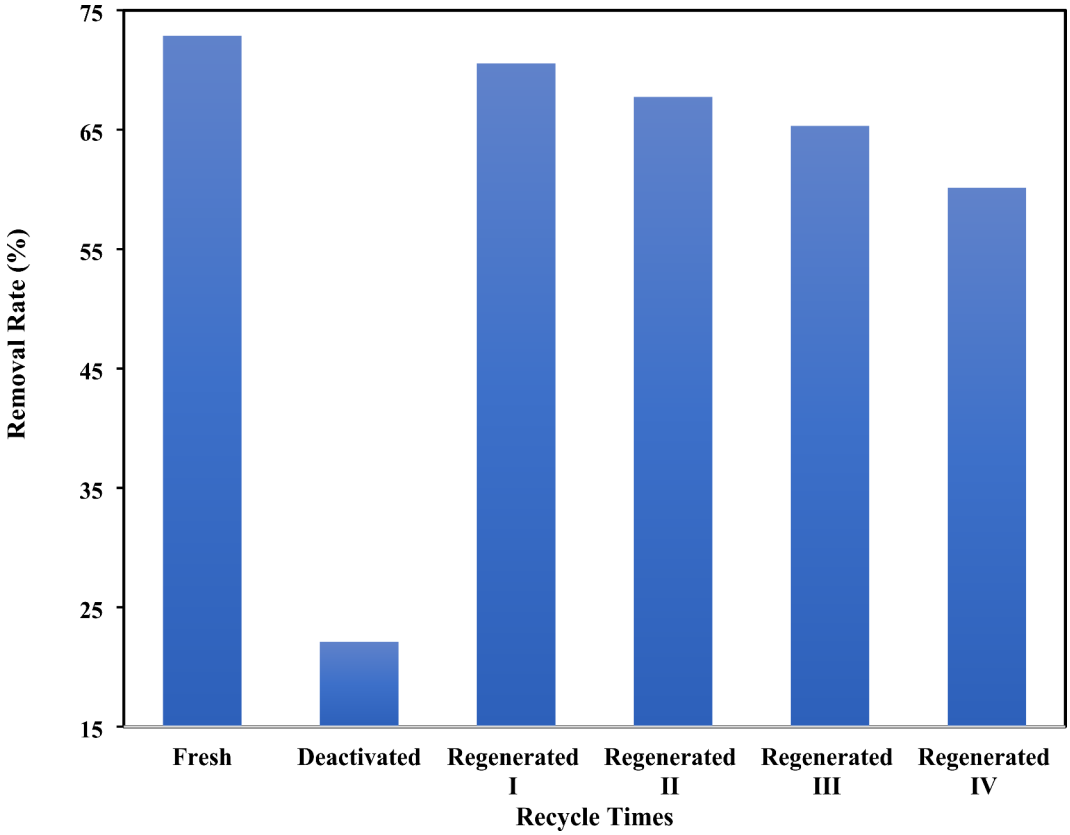

Fig. 13. Recyclability of $Ti_3C_2F_x$-DMSO for Mg^{2+} adsorption.

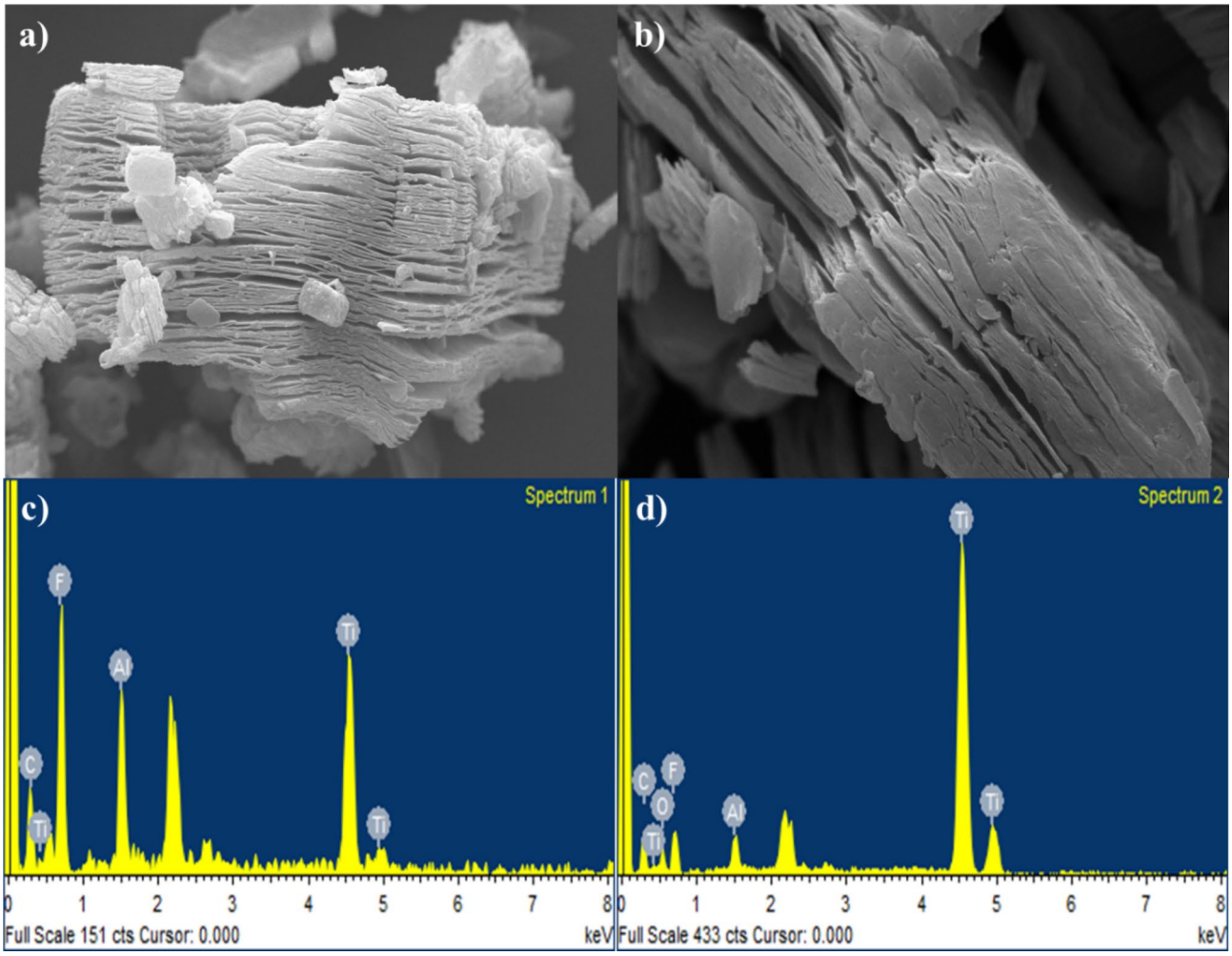

Fig. 14. Recyclability of $Ti_3C_2F_x$-DMSO for Mg^{2+} adsorption.

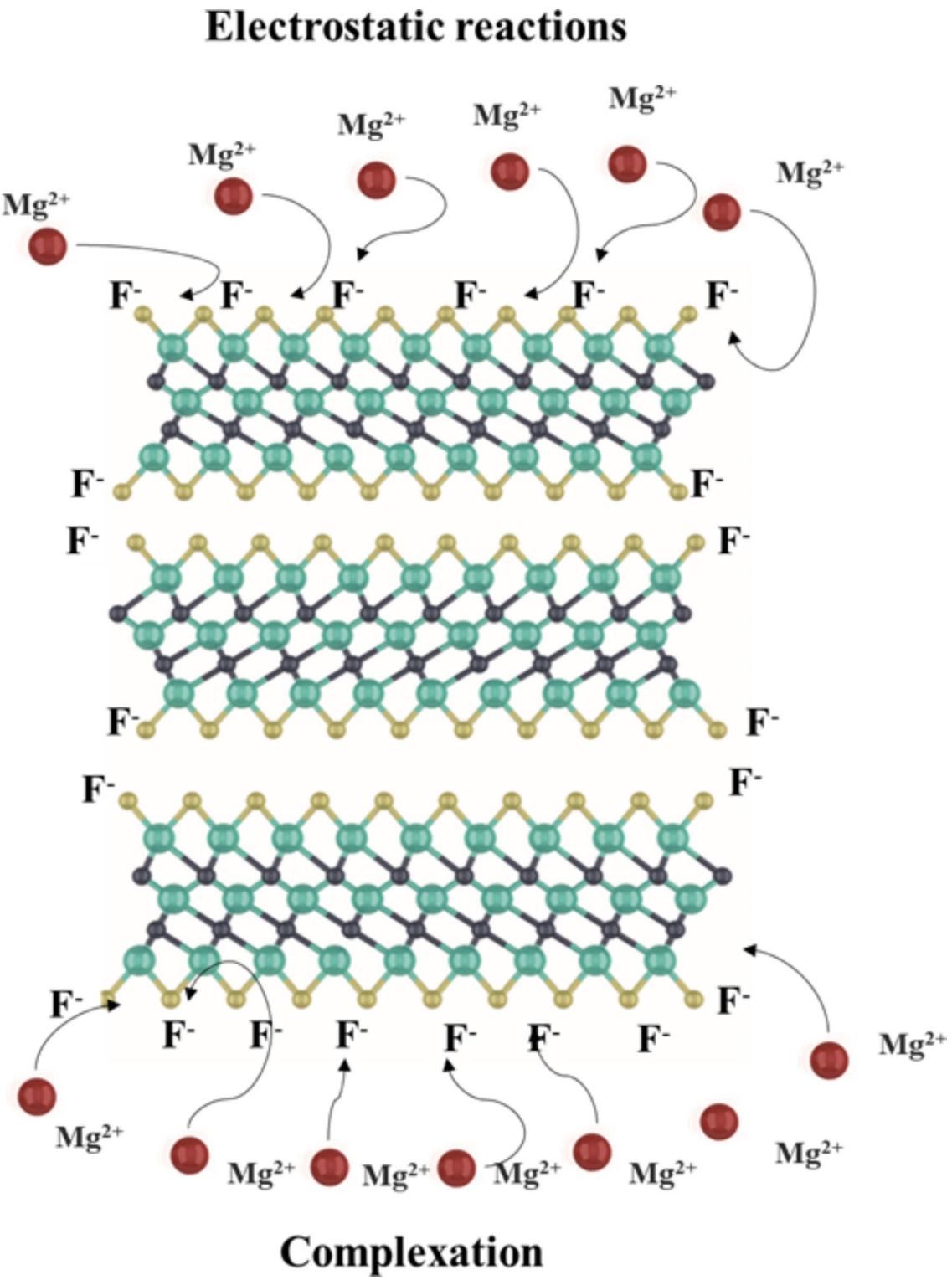

Fig. 15. Mg^{2+} adsorption mechanism by F^- groups on $Ti_3C_2F_x$-DMSO.

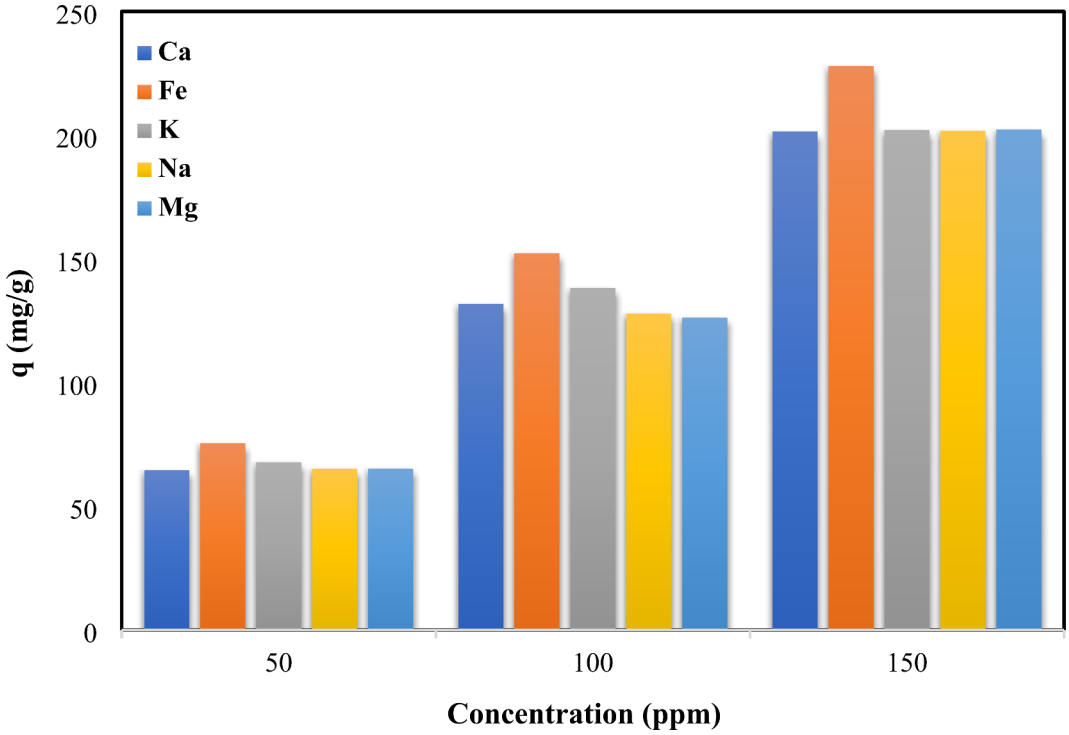

Fig. 16. Effect of competing metal cations on the adsorption of Mg^{2+} by $Ti_3C_2F_x$-DMSO.

Data availability

The datasets used and/or analyzed during the current study are available from the corresponding author upon reasonable request.

Received: 16 July 2024; Accepted: 5 November 2024
Published online: 11 November 2024

References

1. Anasori, B. & Gogotsi, Û. G. *2D metal Carbides and Nitrides (MXenes)* Vol. 416 (Springer, 2019).
2. Naguib, M. et al. Two-dimensional transition metal carbides. *ACS Nano* **6**(2), 1322–1331 (2012).
3. Naguib, M. et al. Two-dimensional nanocrystals produced by exfoliation of Ti3AlC2. *Adv. Mater.* **23**(37), 4248–4253 (2011).
4. Alhabeb, M. et al. Guidelines for synthesis and processing of two-dimensional titanium carbide (Ti3C2T x MXene). *Chem. Mater.* **29**(18), 7633–7644 (2017).
5. Shuck, C. E. et al. Scalable synthesis of Ti3C2Tx mxene. *Adv. Eng. Mater.* **22**(3), 1901241 (2020).
6. Enyashin, A. & Ivanovskii, A. Atomic structure, comparative stability and electronic properties of hydroxylated Ti2C and Ti3C2 nanotubes. *Comput. Theor. Chem.* **989**, 27–32 (2012).
7. Ghidiu, M. et al. Synthesis and characterization of two-dimensional Nb 4 C 3 (MXene). *Chemical Communications* **50**(67), 9517–9520 (2014).
8. Verger, L. et al. MXenes: An introduction of their synthesis, select properties, and applications. *Trends in Chemistry* **1**(7), 656–669 (2019).
9. Hojjati-Najafabadi, A. et al. Magnetic-MXene-based nanocomposites for water and wastewater treatment: A review. *Journal of Water Process Engineering* **47**, 102696 (2022).
10. Rhouati, A. et al. MXene-based electrochemical sensors for detection of environmental pollutants: A comprehensive review. *Chemosphere* **291**, 132921 (2022).
11. Lipatov, A. et al. Effect of synthesis on quality, electronic properties and environmental stability of individual monolayer Ti3C2 MXene flakes. *Advanced Electronic Materials* **2**(12), 1600255 (2016).
12. Ullah, S., et al. Next generation MXene based materials for Electrochemical Sensor: A critical review. *Journal of Molecular Structure* 139830 (2024).
13. Yang, J.-H. et al. Adsorption activities of O, OH, F and Au on two-dimensional Ti2C and Ti3C2 surfaces. *Acta Physico-Chimica Sinica* **31**(2), 369–376 (2015).
14. Zou, X. et al. A simple approach to synthesis Cr2CTx MXene for efficient hydrogen evolution reaction. *Materials Today Energy* **20**, 100668 (2021).
15. Nezami, S., Ghaemi, A. & Yousefi, T. Application of titanium carbide/nitride (MXene)-based NPs in adsorption of radionuclides and heavy metal ions for wastewater remediation: A review. *Case Studies in Chemical and Environmental Engineering* **7**, 100326 (2023).
16. Sindhu, M. et al. Nb-Ta3N5 protected with PANI nanocomposite for enhanced photocatalytic water-splitting towards hydrogen production under visible light irradiation. *Materials Letters* **359**, 135895 (2024).
17. Nazir, M. A., et al. MOF@ graphene nanocomposites for energy and environment applications. *Composites Communications* 101783 (2023).
18. Kumar, J. A. et al. Methods of synthesis, characteristics, and environmental applications of Mxene: A comprehensive review. *Chemosphere* **286**, 131607 (2022).

19. Sheth, Y., et al. Prospects of titanium carbide-based MXene in heavy metal ion and radionuclide adsorption for wastewater remediation: A review. *Chemosphere* 133563 (2022).
20. Bibi, S., et al. MOF/MXene composites: Synthesis, application and future perspectives. *Advanced Sustainable Systems* 2400011 (2024).
21. Wang, L. et al. Synthesis and electrochemical performance of Ti 3 C 2 T x with hydrothermal process. *Electronic Materials Letters* **12**, 702–710 (2016).
22. El-Naggar, M. E. et al. Synthesis, characterization and adsorption properties of microcrystalline cellulose based nanogel for dyes and heavy metals removal. *International Journal of Biological Macromolecules* **113**, 248–258 (2018).
23. Feng, X. et al. Review MXenes as a new type of nanomaterial for environmental applications in the photocatalytic degradation of water pollutants. *Ceramics International* **47**(6), 7321–7343 (2021).
24. Hwang, S. K. et al. MXene: An emerging two-dimensional layered material for removal of radioactive pollutants. *Chemical Engineering Journal* **397**, 125428 (2020).
25. Goel, A., et al. Facile synthesis and characterization of NiCo2O4-rGO binary for energy-storing application. *Journal of Applied Electrochemistry* 1–11 (2024).
26. Nazir, M. A., et al. Recent advances in MXene nanomaterials: Fundamentals to applications in environment sector. *EcoEnergy* (2024).
27. Friedrich, H. E. & Mordike, B. L. *Magnesium Technology* Vol. 212 (Springer, 2006).
28. Kulekci, M. K. Magnesium and its alloys applications in automotive industry. *The International Journal of Advanced Manufacturing Technology* **39**, 851–865 (2008).
29. Poots, V., Mckay, G. & Healy, J. The removal of acid dye from effluent using natural adsorbents—I peat. *Water Research* **10**(12), 1061–1066 (1976).
30. Mordike, B. & Ebert, T. Magnesium: properties—applications—potential. *Materials Science and Engineering: A* **302**(1), 37–45 (2001).
31. Sengupta, P. Potential health impacts of hard water. *International Journal of Preventive Medicine* **4**(8), 866 (2013).
32. Zhao, P. et al. A new paradigm of ultrathin 2D nanomaterial adsorbents in aqueous media: Graphene and GO, MoS 2, MXenes, and 2D MOFs. *Journal of Materials Chemistry A* **7**(28), 16598–16621 (2019).
33. Masoumi, H., Ghaemi, A. & Gilani, H. G. Synthesis of polystyrene-based hyper-cross-linked polymers for Cd (II) ions removal from aqueous solutions: Experimental and RSM modeling. *Journal of Hazardous Materials* **416**, 125923 (2021).
34. Masoumi, H., Ghaemi, A. & Gilani, H. G. Experimental and RSM study of hypercrosslinked polystyrene in elimination of lead, cadmium and nickel ions in single and multi-component systems. *Chemical Engineering Research and Design* **182**, 410–427 (2022).
35. Romano, S. et al. The role of operating conditions in the precipitation of magnesium hydroxide hexagonal platelets using NaOH solutions. *Crystal Growth & Design* **23**(9), 6491–6505 (2023).
36. Raponi, A. et al. Computational modeling of magnesium hydroxide precipitation and kinetics parameters identification. *Crystal Growth & Design* **23**(7), 4748–4759 (2023).
37. Khurshid, H., Mustafa, M. R. U. & Isa, M. H. Adsorption of chromium, copper, lead and mercury ions from aqueous solution using bio and nano adsorbents: A review of recent trends in the application of AC, BC, nZVI and MXene. *Environmental Research* **212**, 113138 (2022).
38. Wang, S. et al. Highly efficient adsorption and immobilization of U (VI) from aqueous solution by alkalized MXene-supported nanoscale zero-valent iron. *Journal of Hazardous Materials* **408**, 124949 (2021).
39. Nezami, S., Ghaemi, A. & Yousefi, T. Efficient removal of radioactive Th (IV) from nuclear wastewater using phosphate-functionalized Ti3C2Tx. *Journal of Environmental Chemical Engineering* **12**(2), 112491 (2024).
40. Chi, Y. et al. Adsorptive removal of radioactive cesium from model nuclear wastewater over hydroxyl-functionalized Mxene Ti3C2T x. *Industrial & Engineering Chemistry Research* **61**(25), 9054–9066 (2022).
41. Rethinasabapathy, M. et al. Amino-functionalized POSS nanocage-intercalated titanium carbide (Ti3C2Tx) MXene stacks for efficient cesium and strontium radionuclide sequestration. *Journal of Hazardous Materials* **418**, 126315 (2021).
42. Ayub, A. et al. A novel Sn/SnOx Ti3C2Tx nanosheet for adsorptive strontium removal in aqueous solution. *Journal of Nuclear Materials* **577**, 154323 (2023).
43. Jun, B.-M. et al. Adsorption of Ba2+ and Sr2+ on Ti3C2Tx MXene in model fracking wastewater. *Journal of Environmental Management* **256**, 109940 (2020).
44. Khoshraftar, Z. et al. Using halloysite nanotubes modified by tetraethylenepentamine for advanced carbon capture: Experimental and modeling via RSM and ANNs. *Chemical Engineering Journal Advances* **16**, 100543 (2023).
45. Ramezanipour Penchah, H., Ghaemi, A. & Ganadzadeh Gilani, H. Benzene-based hyper-cross-linked polymer with enhanced adsorption capacity for CO2 capture. *Energy & Fuels* **33**(12), 12578–12586 (2019).
46. Li, Z. et al. Synthesis and thermal stability of two-dimensional carbide MXene Ti3C2. *Materials Science and Engineering: B* **191**, 33–40 (2015).
47. Jolly, S., Paranthaman, M. P. & Naguib, M. Synthesis of Ti3C2Tz MXene from low-cost and environmentally friendly precursors. *Materials Today Advances* **10**, 100139 (2021).
48. Zeraati, A. S. et al. Improved synthesis of Ti 3 C 2 T x MXenes resulting in exceptional electrical conductivity, high synthesis yield, and enhanced capacitance. *Nanoscale* **13**(6), 3572–3580 (2021).
49. Li, X., Zeng, C. & Fan, G. Magnetic RuCo nanoparticles supported on two-dimensional titanium carbide as highly active catalysts for the hydrolysis of ammonia borane. *International Journal of Hydrogen Energy* **40**(30), 9217–9224 (2015).
50. Peng, Q. et al. Unique lead adsorption behavior of activated hydroxyl group in two-dimensional titanium carbide. *Journal of the American Chemical Society* **136**(11), 4113–4116 (2014).
51. Tang, Y. et al. Enhanced supercapacitive performance of manganese oxides doped two-dimensional titanium carbide nanocomposite in alkaline electrolyte. *Journal of Alloys and Compounds* **685**, 194–201 (2016).
52. Xiang, Y. et al. Preparation of modified sodium lignosulfonate hydrogel–silver nanocomposites. *Polymer Composites* **34**(6), 860–866 (2013).
53. Khan, A. R. et al. Two-dimensional transition metal carbide (Ti 3 C 2 T x) as an efficient adsorbent to remove cesium (Cs+). *Dalton Transactions* **48**(31), 11803–11812 (2019).
54. Sharma, J. P. et al. Evaluating the influence of Ar/N2 flow rate and pressure on the conversion efficiency of a solar-assisted Fe2O3–FeO WS cycle for hydrogen production: A thermodynamic approach. *International Journal of Hydrogen Energy* **52**, 1291–1302 (2024).
55. Xu, Z., Cai, J.-G. & Pan, B.-C. Mathematically modeling fixed-bed adsorption in aqueous systems. *Journal of Zhejiang University Science A* **14**(3), 155–176 (2013).
56. Li, Z. et al. Efficient and sustainable removal of magnesium from brines for lithium/magnesium separation using binary extractants. *ACS Sustainable Chemistry & Engineering* **7**(23), 19225–19234 (2019).
57. Mahmood, M. et al. Nanostructured V2O5 and its nanohybrid with MXene as an efficient electrode material for electrochemical capacitor applications. *Ceramics International* **48**(2), 2345–2354 (2022).
58. Cahyaningrum, S. E. et al. Adsorption of Mg (II) ion from aqueous solution on chitosan beads and chitosan powder. *Journal of Coastal Development* **13**(3), 179–184 (2010).
59. Sepehr, M. N. et al. Removal of hardness agents, calcium and magnesium, by natural and alkaline modified pumice stones in single and binary systems. *Applied Surface Science* **274**, 295–305 (2013).

60. Saeed, A. M. & Hamzah, M. J. New approach for removal of total hardness (Ca 2, Mg 2) from water using commercial polyacrylic acid hydrogel beads, study and application. *International Journal of Advanced Biological and Biomedical Research* **1**(9), 1142–1156 (2013).
61. Din, M. A. U. et al. Synthesis of MXene-based single-atom catalysts for energy conversion applications. *Chemical Engineering Journal* **474**, 145700 (2023).
62. Wang, J. & Guo, X. Adsorption kinetic models: Physical meanings, applications, and solving methods. *Journal of Hazardous materials* **390**, 122156 (2020).
63. Bayazidi, S. et al. Sulfonated crosslinked PVA-CuFe2O4 nanocomposite as a sustainable catalysis for synthesizing antioxidant, antimicrobial, and anti-cancer imidazoles and amino naphthoquinones compounds. *Inorganic Chemistry Communications* **167**, 112743 (2024).
64. Smith, N. D. et al. Thermodynamic properties of Sr-Sb alloys via emf measurements using solid CaF2-SrF2 electrolyte. *Electrochimica Acta* **305**, 547–554 (2019).

Author contributions

Shanli Nezami: Conceptualization, Methodology, Conceived and designed the experiments, Validation, Formal analysis, Investigation, Resources, Writing—original draft, Writing—review & editing. Ahad Ghaemi: Conceptualization, Methodology, Software, Conceived and designed the experiments, Validation, Formal analysis, Investigation, Resources, Data curation, Writing—original draft, Writing—review & editing, Supervision Visualization, Project administration Taher Yousefi: Conceptualization, Validation, Formal analysis, Investigation, Resources, Data curation, Writing—review & editing.

Competing interests

The authors declare no competing interests.

Additional information

Supplementary Information The online version contains supplementary material available at https://doi.org/10.1038/s41598-024-78942-x.

Correspondence and requests for materials should be addressed to A.G.